Nanoengineering of non-aqueous liquid electrolyte solutions for future lithium metal batteries

Dominik Weintz[1], Martin Werres[2,3], Birger Horstmann[2,3], Rachid Amine[4] ✉, Chi-Cheung Su[5], Xinlin Li[5], Yaobin Xu[6], Ridwan A. Ahmed[6], Wu Xu[6], Chongmin Wang[7], Bastian von Holtum[8], Simon Wiemers-Meyer[8], Dongliang Chen[9], Jianwei Lai[9], Feifei Shi[9], Sascha Berg[1], Egbert Figgemeier[1], Christian O. Plaza-Rivera[10], Daniel Wang[11], Yang Shao-Horn[10,11,12], Aravind Unni[13], Ulrike Krewer[13], Stephen Scoggins[14], Perla B. Balbuena[14,15,16], Jorge M. Seminario[14,15,17], Asia Sarycheva[18], Ziyuan Lyu[3,19], Dominic Bresser[3,19], Florian Hausen[20,21], Rüdiger-A. Eichel[20,21], Khalil Amine[5,22], Arnulf Latz[2,3] ✉, Robert Kostecki[18] ✉, Martin Winter[1,8] & Isidora Cekic-Laskovic[1] ✉

Research and development of non-aqueous electrolyte solutions are essential for practical advancement towards the production of high-energy lithium metal batteries (LMBs). An ideal LMB electrolyte solution should enable highly efficient, uniform and prolonged lithium metal plating and stripping, preserve the electrodes' electro(chemo)mechanical properties and ensure compatibility with all cell components. However, despite extensive research efforts, scientists have yet to achieve an electrolyte design that meets these requirements simultaneously. Here, by examining the nanoengineering aspects of various non-aqueous electrolyte solution designs, we elucidate the understanding of the nanoscale physicochemical and electrochemical processes taking place in LMBs, which are mainly governed by the thermodynamic and kinetic properties of the electrolyte system. We also explore emerging research directions and propose an accelerated, iterative framework that integrates nanoengineering principles with machine learning, high-throughput computation and experimentation to facilitate the development of next-generation non-aqueous electrolyte solutions for practical LMBs.

The growing demand for portable electronic devices and the shift to electric transportation have driven efforts to improve state-of-the-art lithium-ion battery (LIB) technology (where the negative electrode is generally graphite based), targeting higher energy density and longer lifespans. Metallic lithium is the ideal negative electrode material due to its high theoretical capacity (3.86 Ah g^{-1} and 2.06 Ah cm^{-3}) and low redox potential (−3.04 V versus standard hydrogen electrode at 25 °C)[1,2]. Despite over a century of research (Fig. 1), the widespread adoption of rechargeable lithium metal batteries (LMBs), which use metallic lithium as the negative electrode, is still hindered by safety concerns and short cycle life[3–5]. To address these challenges, research efforts are focused on developing non-aqueous electrolyte solutions that enable highly reversible plating and stripping of Li metal at the LMB negative electrode in a compact and uniform manner, while protecting it from degradation and ensuring compatibility with the other cell components. The formation, composition and structure

A full list of affiliations appears at the end of the paper. ✉e-mail: aminer@anl.gov; Arnulf.Latz@dlr.de; r_kostecki@lbl.gov; i.cekic-laskovic@fz-juelich.de

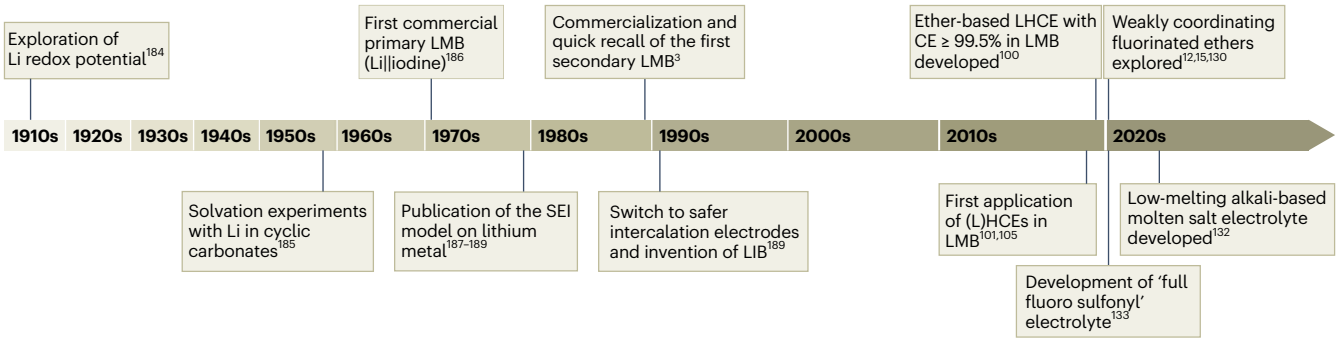

Fig. 1 | Chronological development of LMBs. Key historical milestones and technological advancements in the development of LMB technology. The superscript numbers refer to the corresponding references[184–189].

of the protective layer formed at the negative electrode|electrolyte interface—the solid electrolyte interphase (SEI)—are crucial parameters in determining an LMB's performance and cycle life[6,7]. Unlike the case in Li^+ host materials such as graphite, conventional organic carbonate-based electrolyte solutions fail to effectively protect Li metal electrodes, because the SEI formed is organic rich and promotes uneven Li deposition and continuous interphase growth. This leads to a series of detrimental mechanisms, such as accelerated electrolyte consumption, Li inventory loss, formation of 'dead' Li (i.e., Li metal regions that are electronically disconnected from the current collector) and growth of the cell's impedance[4,8]. High-performing liquid electrolyte solutions for LMBs ideally form a homogeneous, inorganic-rich SEI with fast reformation/repair kinetics, capable of adapting to the mechanical stress occurring during the cell's galvanostatic cycling and promoting the formation of compact Li deposits[9,10]. The ability of a liquid electrolyte solution to form an effective SEI is primarily determined by the Li^+ ion solvation sheath and the binding strengths between the electrolyte's components. While cyclic carbonates such as ethylene carbonate (EC) tend to interact strongly with the solvated Li^+ ions, weakly binding solvents and high salt concentrations (>3 M)[11] lead to the formation of contact-ion pairs (CIPs) and aggregates (AGGs), where the salt-derived anion actively participates in the inner Li solvation shell. This molecular arrangement promotes the reduction of the anion rather than the solvent, resulting in the formation of a beneficial, inorganic-rich SEI. This is why most high-performing liquid electrolyte solutions for LMBs adopt this solvation design[9,12–16]. However, further technological advancements are needed to develop LMBs that match and ideally outperform the current state-of-the-art commercial LIBs.

In this Review, we elucidate the thermodynamic and kinetic properties of non-aqueous liquid electrolyte solutions, focusing on Li salt concentrations and solvation strength effects on the Li^+ ion solvation shell. We also discuss how this class of electrolyte affects electro(chemo)mechanical properties of the SEI and how to promote the formation of an ideal Li metal surface interphase, evaluating the most recent research on the design of performance-determining interphases. We also explore beyond state-of-the-art electrolyte solution concepts and design strategies to achieve the ideal electrolyte and SEI-forming conditions. Finally, we focus on the use of analytical methods to understand how to optimize the most promising electrolyte concepts for future LMB development.

Fundamental properties of non-aqueous Li-containing liquid electrolyte solutions

The complex solvation environment of Li ions affects the electrolyte solution's dynamics, including interface kinetics, transport and thermodynamic properties. Conventional metrics, such as the dielectric constant ε_r and the donor number (DN), are used to evaluate solvent–ion interactions, providing a macroscopic view of a solvent's ability to dissociate salts and solvate ions, and serving as the basis for designing new electrolyte formulations[17]. On the one hand, high ε_r and DN of the solvents (usually DN > 10 kcal mol^1, $\varepsilon_r > 5$) and low DN of the salt-derived anion are required to enable sufficient dissociation of the conducting salt; however, to promote the often desired ion–ion interactions in the electrolyte's solvation structure, lowering of the $DN_{solvent}$-to-DN_{anion} ratio is required[18]. The electrochemical stability window (ESW), defined as the range of applied potentials between the reduction and oxidation limits of the electrolyte solution, is also a crucial parameter. To roughly estimate the ESW, a molecular-orbital-based analysis can be carried out by examining the energy gap between the highest occupied molecular orbital and the lowest unoccupied molecular orbital of the solvent[19]. However, this theoretical evaluation is based solely on an isolated single solvent molecule and may deviate from experimental ESW measurements. Indeed, ionic interactions in the electrolyte solution can influence the energy gap between highest occupied molecular orbital and lowest unoccupied molecular orbital[20]. Despite its limited accuracy, this approach still provides easy-to-obtain estimations that can approximately indicate the reduction and oxidation limits of a practical electrolyte solution. Nevertheless, the ESW theoretical evaluation must always be validated via electrochemical measurements such as linear or cyclic voltammetry[21].

Transport properties

Ionic conductivity is a key transport property of electrolyte solutions, indicating how easily ions move to participate in electrochemical reactions, thereby considerably influencing the cell's power output and the Li deposition morphology at high currents.

Since the reactions at the electrodes in LMBs depend on the Li^+ transport, it is crucial to quantify the Li^+ contribution to overall ionic conductivity. The two critical transport properties here are the transport number (t) and the transference number (T)[22]. Although often used interchangeably, they are fundamentally different: the transport number quantifies the relative mobility of each ionic species (e.g., Li^+ and $[Li_2X]^+$), whereas the transference number measures the net transference of all Li^+-containing species. In most moderate-concentration liquid electrolyte solutions, with approximately 1 M salt concentration, the Li^+ transference number is more relevant to cell chemistry and usually hovers around 0.3, indicating that most current is carried by the anions[11,23,24]. This parameter is highly influenced by the solvation structure; thus, higher fractions of CIPs generically lead to lower transference numbers, while AGG structure can promote fast charging performance. An adequate measurement of this parameter remains challenging; however, combining electrochemical methods with complementary techniques, such as nuclear magnetic resonance (NMR), provides a precise and accurate evaluation of the transference number[25–28].

Thermodynamic properties

Although ε_r and DN are commonly used to assess solvation strength, they do not fully capture the complex ion–ion and ion–dipole

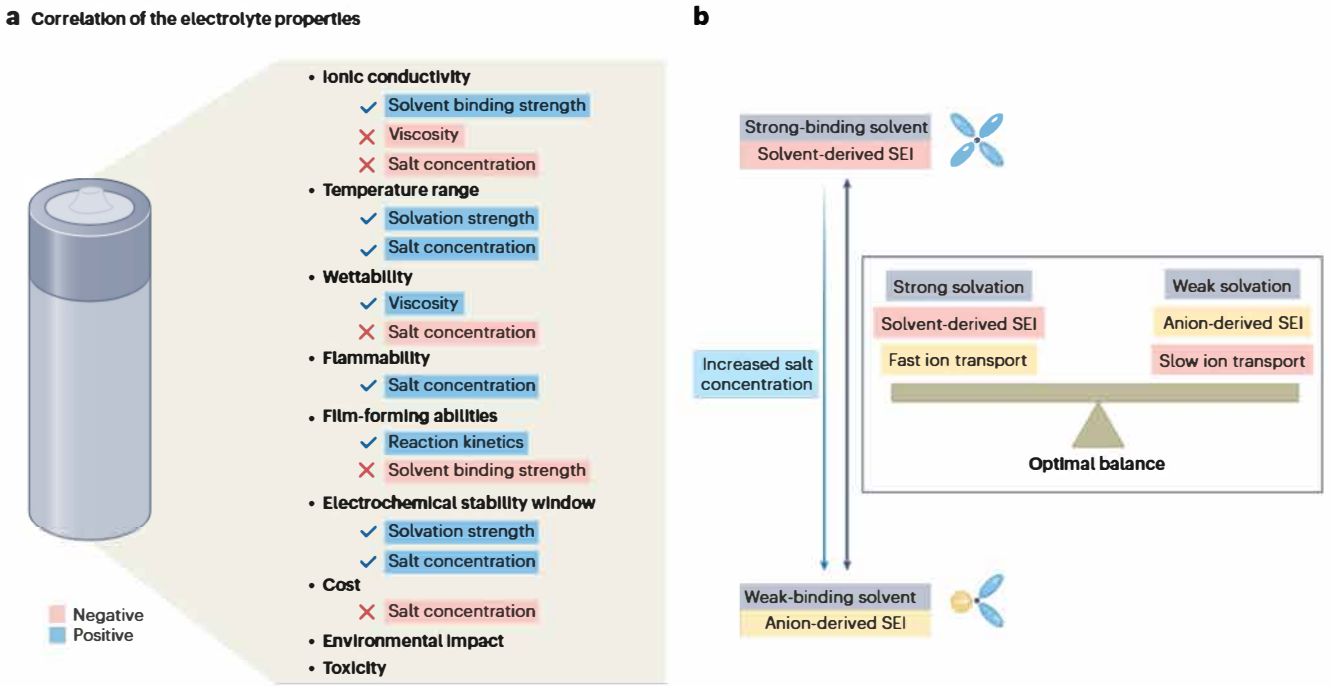

Fig. 2 | Interplay between essential electrolyte properties. a, Non-aqueous liquid electrolyte solution properties (black) and the major influencing factors. Blue indicates a positive and red indicates a negative correlation of the electrolyte property and its underlying impact factor. Viscosity refers to both the dynamic and kinematic viscosity. **b**, Anticorrelation between the electrolyte's electrochemical stability and ionic conductivity based on the solvent solvation strength. Panel **b** adapted from ref. 12, Springer Nature Limited.

interactions in conventional non-aqueous lithium-containing electrolyte solutions. These solutions usually consist of a mixture of free solvents, solvent-separated ion pairs, CIPs and AGGs. To understand electrolyte solvation structures, it is crucial to quantify the Gibbs free energy, entropy and enthalpy changes of ion-pair solvation, which reflect the competition and equilibrium among ionic species[29]. These crucial thermodynamic metrics, often determined through calorimetry and electrochemical measurements, are rarely reported for battery cell electrolytes, despite their significance for essential cell parameters such as ionic conductivity and $Li^+|Li$ redox potential. A deeper understanding of these macroscopic thermodynamic properties is essential to link them to the microscopic ion-pairing dynamics, including Li^+↔anion association and Li^+↔solvent dissociation[30–32].

Interface phenomena

Interfacial simulations extend beyond the conventional analysis of bulk electrolyte properties. By combining classical molecular dynamics, tight-binding simulations and density functional theory (DFT) calculations, researchers investigate how multicomponent liquid electrolyte solutions interact within the electrical double layer (EDL) formed on the electrode surface and provide predictions of potential reduction pathways at the electrode|electrolyte interface. The results indicate that for anions to effectively participate in SEI formation they must be present in the EDL and the lithium-ion solvation sheath (CIPs or AGGs)[33]. Additional outcomes of interfacial simulations are provided by the first-principles-based analysis of changes in solvation structures and their effects on (de-) solvation barriers at interfaces. By analysing cation diffusion, desolvation and deposition pathways for various liquid electrolyte solutions, researchers can gain further insights into the possible transport and electrodeposition barriers from a given electrolyte near the electrode surface. These barriers arise from the competition between solvation forces and solvent electron affinity towards the electrode surface[34].

Impact of solvent chemistry and salt concentration

Two major solvent groups can be identified for Li-based electrolyte solutions, each offering an adequate combination of essential physicochemical, electrochemical and thermal properties (Fig. 2a). Cyclic organic carbonates (e.g., EC), commonly used in commercially available LIBs, possess comparably high dynamic viscosity, high oxidative stability (>4.5 V versus $Li|Li^+$ with an inert electrode) and high binding strengths toward the Li^+ ions. Ethers (e.g., tetrahydrofuran, 1,2-dimethoxyethane (DME)), on the other hand, generally exhibit lower dynamic viscosities ($\eta_{20°C}$(DME) = 0.42 mPa s versus $\eta_{20°C}$(EC) = 1.92 mPa s) and higher reductive stability (DME, 0.3 V versus $Li|Li^+$; EC, 1.0 V versus $Li|Li^+$) than their cyclic carbonate counterparts, making them more compatible with a Li metal electrode[9,35].

High-concentration electrolyte (HCE) solutions are intensively investigated, especially for use in LMBs. Increasing salt concentration from 1 M to ~4–6 M causes a shift from solvation structures dominated by solvent-separated ion pairs, typically found in moderate-concentration electrolytes (MCEs; 1 M < electrolyte concentration < 3 M; the exact boundaries may differ on the basis of the context and the components involved), to CIPs and AGGs, characterized by strong ion–ion and solvent–ion interactions[36]. This alteration in the molecular arrangements changes some crucial properties of the electrolyte solution. (1) Due to the stronger solvent–ion interactions, the ESW widens, increasing the stability of the solvent against reduction, which promotes the formation of a favourable and effective anion-derived inorganic SEI[13]. (2) The widened ESW increases the oxidative stability of the solvent, making even oxidatively fragile ethers such as DME usable with most 4-V-class positive-electrode chemistries[37]. (3) Beyond a certain salt concentration threshold, the transport properties of the ions change fundamentally. Instead of the usually observed ion transport via the 'vehicle-type' mechanism based on diffusion, researchers propose a Li^+ ion hopping mechanism experimentally proven in certain HCEs, where the solvating moieties of the solvent and anion bridge different Li^+. This allows Li to hop between different Li coordination sites, resembling a diluted form of molten salt[38,39].

Although the increase in dynamic viscosity decreases the bulk ionic conductivity of the electrolyte solution, the high salt concentration prevents the rapid depletion of Li^+ ions near the electrode|electrolyte interface, enabling homogeneous Li plating even at high currents[13]. Another approach to favour the formation of CIPs and AGGs is using weakly solvating solvents, such as fluorinated 1,2-diethoxyethane and its derivatives and sterically demanding solvents, which promote the formation of favourable anion-derived interphases even within the standard 1–1.2-M concentration range[12,40]. Electrolytes containing weakly coordinating ethers and HCEs exhibit substantial energy barriers to ion transport near the negative-electrode surface. In such systems, the anions possess a high electron affinity towards the Li metal electrode, promoting the rapid deposition of inorganic SEI products on the surface[36]. However, the low solvation strength hinders the ion mobility; therefore, achieving an optimal balance between solvation properties and ion transport is essential to developing electrolyte solutions capable of enabling sufficient power density during cell operation, while also promoting the formation of an effective anion-derived Li metal SEI (Fig. 2b)[12].

Solid electrolyte interphase

The SEI, produced during the cell's formation cycles, serves as a protective, passivating layer on the negative electrode, preventing further irreversible reactions between the electrode and the electrolyte, and usually consists of fully reduced inorganic species in the proximity of the Li metal electrode surface and organic species in the outer SEI, often arranged in a mosaic-like structure. Researchers also report the formation of amorphous and multilayer interphases for specific electrolyte formulations and galvanostatic cycling conditions[6]. Nucleation and growth of the SEI are primarily based on an electron tunnelling model with a self-limiting thickness of 2–3 nm, which deviates from the experimentally determined values ranging from 6 to >50 nm (refs. 41–44). The mechanism for further growth beyond the critical tunnelling thickness[41,45] remains elusive; however, scientists propose several mechanisms to explain this excessive SEI growth[46], including electron diffusion through point defects such as Li interstitials[47,48], solvent diffusion[49,50], electron conduction through the SEI layer[49,50] and transition-metal-enabled electron transfer, whereby the transition metals originate from the positive electrode and deposit on the negative electrode[51]. For zero-excess (also called anode-free or anodeless) LMBs, the SEI forms on an electronically conductive substrate, typically a Cu electrode, during the first cell's cycle before Li deposition occurs. However, for LMBs with a Li metal negative electrode, the Li metal is covered by a native passivation layer that forms during handling in the atmospheric environment[52,53]. The native passivation layer, mainly composed of Li_2CO_3, LiOH and Li_2O, influences the formation and composition of the SEI upon electrolyte contact. Even after several cell cycles, the effect of the native passivation layer on the SEI, Li deposition morphology and cell performance remains[54,55]. Surface irregularities of the Cu electrode, including microcracks and oxide layer formation, can promote heterogeneous Li deposits[56]. Besides these features, several other parameters can influence the SEI properties, including the electrolyte formulation (i.e., type of salt anion[57], solvent[58] and use of additives[59]), applied current[60], operating cell potential[61], type of counter-electrode used[62], pressure applied during galvanostatic cycling[63], type and number of separators used during cell assembly[64] and operating temperature[65,66] (Fig. 3a).

Mechanical properties

During cell operation, the theoretically infinite volume changes of the hostless Li metal electrode, depending on the reversible Li metal thickness variations[43,67], can lead to cracks in the SEI. These cracks expose reactive (i.e., with no passivated surface) Li metal to the electrolyte, highlighting the importance of the SEI's mechanical properties in LMBs. The ideal mechanical properties of the SEI are, however, seemingly contradictory: for two-dimensional plating a high elastic modulus is desirable, while to mitigate cracking a flexible SEI is desirable, which can also be achieved by high mechanical strength and high ductility[2,68]. Several research groups have investigated the elastic modulus of the SEI formed in different electrolyte solutions, ranging from 0.3 GPa for organic carbonate-based formulations up to over 5 GPa in HCEs and ether-based electrolytes[44,69]. Simulations and experimental data indicate that elastic moduli of over 3 GPa result in adequate SEI stability, and elastic moduli exceeding that of Li (4.9–7.8 GPa) partially suppress the formation of needle-like Li electrodepositions like whiskers[69–71]. Recent studies indicate that optimizing the elastic modulus and elastic strain limit for maximizing elastic deformation energy is crucial to further improve the stability of the SEI as well as the cell's Coulombic efficiency (CE). This suggests a multilayer interphase layer that incorporates both rigid inorganic and flexible organic components as the ideal SEI structure to accommodate volumetric changes during lithium plating and stripping (Fig. 3a)[72–74]. The adhesion strength of the SEI to the Li metal is another critical parameter in impacting the Li deposition morphology, as a high interface strength (e.g., at the LiF–Li interface) mitigates the formation of mossy-like Li electrodepositions[75].

Ionic and electronic transport properties

Understanding the SEI requires knowledge of electronic and ionic conduction mechanisms. Their investigation is challenging due to the SEI's nano- to submicrometric thickness, fragile nature and lack of suitable analytical techniques. The excess of interstitial Li^+ ions is identified as a possible charge carrier in the SEI inorganic layer. Here, the charges are transported via a knock-off mechanism through the crystal's inorganic lattice, and mesoscale modelling reveals that diffusion in the SEI follows the structural layered pattern, switching from knock-off to pore diffusion in the outer layer[76,77]. The knock-off mechanism has been further investigated by combining in situ liquid secondary ion mass spectroscopy (SIMS) with transmission electron microscopy (TEM) measurements on an isotope-labelled SEI[78]. Other reports have demonstrated ion transport through SEI grain boundaries, highlighting the need to understand nanoscale SEI growth and crystal interface formation[79,80]. Recently, Xu et al.[81] developed an in situ biasing TEM method for directly measuring the electrical properties of SEI layers. Contrary to earlier assumptions, the SEI layers exhibit semiconducting rather than insulating behaviour, supporting analogous theoretical simulations (Fig. 3b)[81–84]. It is demonstrated that a high proportion of organic components in the SEI generates a substantial amount of porous structure. Moreover, the presence of charged molecular fragments, organic radical species and large numbers of dissolved Li^+ ions may lead to the formation of electrochemically inactive dead Li metal[81]. In this case, dead metallic Li particles remain unstripped in the SEI layered structure and are electronically isolated from the current collector and Li metal negative electrode. Similar to ion conduction, grain boundaries between SEI compounds can enhance electron transport in the SEI[85]. Since the SEI's inner layer is a composite of crystalline particles (including organic and inorganic species) in an amorphous matrix, electron leakage and ion transport are governed by the continuous amorphous phase.

Lithium deposition morphology

A major cause of LMBs' short cycle life and safety risks is associated with the Li electrodeposition morphology. Indeed, inhomogeneous Li deposits increase the surface area at the electrode surface and promote Li-consuming irreversible reactions[2]. The Li deposition morphology can be distinguished in favourable compact low-surface-area deposits and high-surface-area lithium or mossy-like deposition morphologies, such as Li whiskers and Li dendrites (Fig. 3c). High-surface-area lithium morphologies are linked to the low cell CE, due to increased

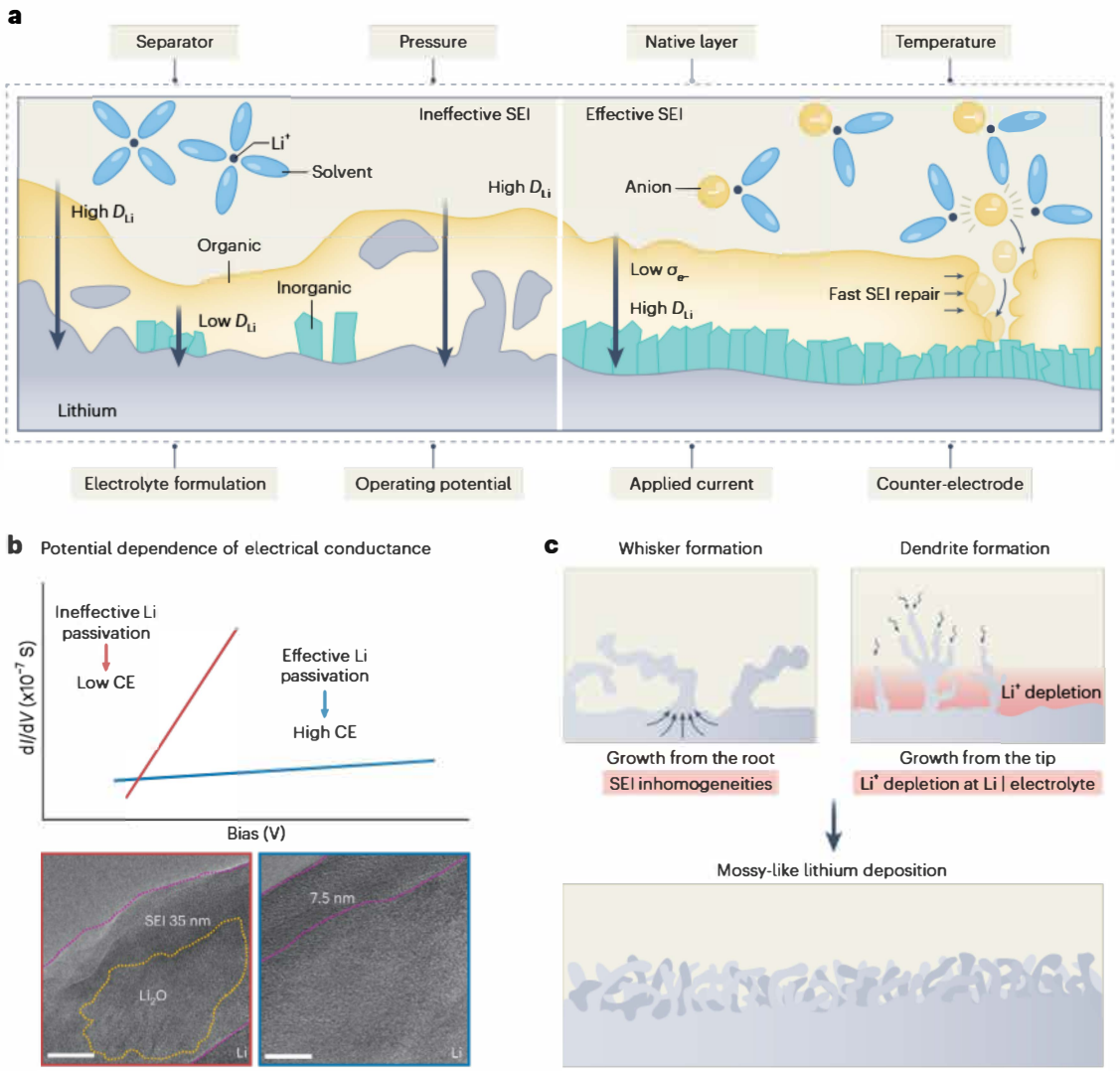

Fig. 3 | SEI on lithium metal and origin of mossy-like Li deposition. **a**, Comparison between an ineffective protective SEI (left) and an effective protective SEI layer (right), surrounded by the major impact factors during SEI formation. D_{Li}, lithium diffusion coefficient; σ_e, electrical conductivity. The ineffective SEI is characterized by an inhomogeneous distribution of SEI components, leading to variations of Li diffusion across the interphase. In contrast, an effective SEI layer usually consists of a homogeneous multilayer structure with a layer rich in rigid, inorganic components (e.g., LiF, Li_2O) close to the electrode covered by a flexible organic layer. **b**, Differential electrical conductance (d*I*/d*V*–*V* curve) of two differently derived SEIs. The atomic structure of the corresponding SEI layers on the Li deposits is derived from ineffective (SEM micrograph within the red border) and effective (SEM micrograph within the blue border) passivating electrolyte solutions. **c**, Schematic illustration of mossy-like Li deposition, including its origins. (1) Inhomogeneities of the SEI cause preferential Li nucleation sites, leading to the formation of root-grown lithium whiskers. (2) When the Li plating rate outpaces ion diffusion in the liquid electrolyte, the Li^+ concentration at the Li metal|liquid electrolyte interface drops. At the point of Li^+ depletion at the negative electrode, also known as Sand's time, fractal-like Li dendrites grow from the tip[60]. Panel **b** adapted from ref. 81, Springer Nature Limited.

side reactions, and the formation of dead Li[71,86]. Typically, dendrites only form above the limiting current density after Sand's time due to a depletion of ions near the electrode surface, and are thereby limited by the electrolyte and ion mobility[60]. On the other hand, mossy Li and Li whiskers arise from an ineffective SEI formation[87,88]. The electronic properties are of high importance as the deposited Li particles exhibit a wide size distribution, large fractions of dead Li and a high topographical tortuosity at high rates of differential electronic conductions[81]. Equally important is the SEI homogeneity to ensure uniform Li plating, as minor inhomogeneities and cracks can lead to Li whisker growth due to local stress and current hotspots[89]. Several studies have correlated the charge-transfer and SEI formation kinetics with the Li deposition morphology, assuming that fast repair kinetics promote compact Li deposition morphology[10,90,91]. Recent mesoscale kinetic Monte Carlo simulations further revealed that clogging of the grain boundaries due to extensive SEI growth causes spatial variations and kinetic limitations in Li^+ ion transport, promoting the growth of Li whiskers and heterogeneous Li deposits[92,93].

Optimizing the SEI layer to attain optimal electronic resistance, ionic conductivity, mechanical strength and flexibility might seem contradictory. In this context, LiF is regarded as the ideal inorganic SEI component due to its high mechanical strength and electronic resistance. For this reason, considerable research efforts have been devoted to increasing the LiF content in the SEI[90,94,95]. Given the complex nature and broad range of desired SEI properties, effective Li protection may require more than increasing the often highly praised LiF content, as other inorganic compounds such as Li_2O also beneficially affect the cell's CE, even without using fluorinated solvents in the electrolyte solution[96]. Moreover, the presence of electronegative fluorine- and oxygen-rich functional groups in the electrolyte components is known

to improve the SEI formation kinetics and promote faster and more uniform SEI repair (Fig. 3a)[10].

Advances in analytical techniques and the predictive power of computational methods could also facilitate meaningful correlations between key SEI parameters.

Liquid electrolyte solutions for LMBs

Various nanoengineered liquid electrolyte solutions have been proposed in the literature to meet the demanding requirements of the Li metal negative electrode while simultaneously ensuring good compatibility with state-of-the-art positive-electrode chemistries operating at high cell potentials (i.e., >4 V)[1,9,97]. In this section, we discuss some of the most important concepts of electrolyte development.

Localized HCEs

HCEs are considered promising alternatives to conventional MCEs for the future development of LMBs[98,99]. However, they show drawbacks such as high dynamic viscosity, low ionic conductivity, poor wettability of separators and thick electrodes, as well as high costs. Adding a non-solvating liquid additive, i.e., a diluent, to an HCE produces so-called localized high-concentration electrolytes (LHCEs), which have demonstrated substantial improvements in the electrochemical performance of LMBs compared with HCE and organic carbonate-based MCE solutions[100–102]. LHCEs have substantially lower dynamic viscosity, improved wettability and lower costs compared with their HCE counterparts[7]. As the favourable inner solvation sheath of Li^+ ions, consisting of CIPs and AGGs, remains largely unchanged, most benefits of an HCE persist[103,104]. According to the design principle, an effective LHCE requires a diluent with low dynamic viscosity, low-to-zero solvating capability of the conducting salt (DN ≤ 10), sufficient miscibility with the solvating solvent and a broad ESW[105,106]. Designing an ideal LHCE depends on the precise combination and amounts of the conducting salt, solvent and diluent[107]. Since the first report on LHCEs, researchers have successfully designed various LHCE solutions that considerably enhance the electrochemical performance of various Li-based cell chemistries[100,101,108–111]. The peculiar design of LHCEs promotes the formation of larger, more uniform, and compact Li electrodeposits in LMBs, leading to higher cell CE compared with others using HCEs and MCEs[109,112]. A typical LHCE reported for LMBs in the literature comprises lithium bis(fluorosulfonyl)imide (LiFSI) salt in DME solvent diluted by 1,1,2,2-tetrafluoroethyl-2,2,3,3-tetrafluoropropyl ether (TTE) (1:1.2:3 by mol), which enables an average CE of 99.5% (Fig. 4a; all CE values are determined in Li‖Cu cells with current densities of ≥0.5 mA cm^{-2} between 20 and 25 °C if not stated otherwise), yields compact, granular Li deposition and outperforms several LHCEs containing other solvating solvents and diluents under the same conditions[100,113]. Thus, it enables long-term cycling stability with a $LiNi_{0.6}Co_{0.2}Mn_{0.2}O_2$ electrode under practical conditions, i.e., over 600 cycles with 76% capacity retention in an application-oriented 350 Wh kg^{-1} LMB, demonstrating good passivating behaviour on both the negative and positive electrodes[114]. Researchers have investigated other highly fluorinated ethers as diluents because they satisfy most of the requirements. Further studies have demonstrated that diluents with weak solvating capabilities in LHCEs enhance the LMB performance, as such diluents can partially participate in the solvation structure, reduce the solvation strength of the solvent and contribute more to the formation of thin yet robust interphases[115,116]. Examples of such weakly coordinating diluents include bis(2,2,2-trifluorothyoxy)methane (BTFM)[117], 1,1,2,2-tetrafluoro-3-methoxypropane[118], 2,3-difluoroethoxybenzene[95] and 1,2-bis(1,1,2,2-tetrafluoroethoxy)ethane[119,120]. The coordination strength is primarily determined by the number of ether groups and the fluorination of α-carbons. Mono-ether TTE shows minimal ion coordination, whereas bi-ether BTFM, lacking fluorinated α-carbons, participates in lithium's inner solvation shell, further promoting CIP and AGG formation (Fig. 4b). Various solvent classes are also used in LHCEs to improve specific properties of Li metal cells. For instance, LHCEs with triethyl phosphate or ionic liquids provide flame-retardant properties. Replacing DME with triethyl phosphate slightly lowers the cell's CE to 99.2%, while ionic-liquid-based LHCEs maintain CEs comparable to those of Li metal cells with ether-based electrolyte systems[121,122].

Recent advances in LHCEs have led to the development of electrolytes with unique properties (e.g., micelle-like solvation sheaths), further improving specific performance parameters of LMBs[103,104,123–126]. To address inadequate Li metal cell cycling performance at high-rate currents, Kim et al. developed a high-entropy electrolyte with five solvents and diluents, showing a high ionic conductivity (>3 mS cm^{-1}; ionic conductivities are measured at 20–25 °C if not stated otherwise) owing to its solvation cluster structures, which enable efficient cell operation at current densities of >1 mA cm^{-2} (Fig. 4b)[127]. Yang et al. recently proposed a supersaturated electrolyte solution (16 mol l^{-1}) prepared by dissolving 2 M LiFSI in a 1:7 DME/2,2-dichlorodiethylether (ClDEE) mixture. The resulting Li^+–FSI^- tight ion clusters enhance reductive stability and promote fast, inorganic-rich SEI formation, achieving over 99.8% average CE and stable operation of a 510 Wh kg^{-1} Li‖$LiNi_{0.8}Co_{0.1}Mn_{0.1}O_2$ 5.6-Ah pouch cell across 116 cycles at low current rates with 84% capacity retention (Fig. 4a)[16].

Weakly solvating electrolytes and molten salts

Besides LHCEs, MCEs with fluorinated derivatives of well-known solvents are also studied for possible LMB applications. The introduction of electron-withdrawing groups (e.g., fluoro groups) increases the oxidative stability of the electrolyte solution, ensures compatibility with high-potential positive electrodes and promotes an anion-derived inorganic SEI with improved formation kinetics (Fig. 4b)[128,129].

In particular, targeted ether fluorination represents a promising approach, aiming to optimize both the degree and positional placement of fluorine relative to the ethereal oxygen, thereby balancing redox stability, solvation strength and ionic conductivity[12,130]. In DME and its derivatives, the ether groups in the ethylene oxide segment solvate Li^+ ions through a five-member ring configuration, which offers good solubility and facilitates cation–anion separation. The targeted introduction of electron-withdrawing functional groups ($-CF_3$, $-F$) can modulate the electronic properties while retaining the favoured five-member-ring solvation structure. For example, 2-[2-(2,2-difluoroethoxy)ethoxy]-1,1,1-trifluoroethane, 1-(2,2,2-trifluoro)-ethoxy-2-methoxyethane and 1,1,1-trifluoro-2,3-dimethoxy-propane exhibit the optimum binding strength to the Li^+, favouring a cell CE of up to 99.6% while maintaining a high ionic conductivity of >4 mS cm^{-1} (20–25 °C)[12,14,117]. Several fluorinated mono-oxygen ethers have also been proposed as electrolyte solvents, with the symmetric difluorinated diethyl ether (BFE) enabling highly efficient lithium plating/stripping with a high average CE of 99.75% (Fig. 4a)[15]. Recently, a biphasic electrolyte formulation was reported comprising a TTE-based organic phase paired with a water-in-salt solution with 12-crown-4 ether and tetraglyme as ionophores. In this electrolyte system, Li^+ forms CIP- and AGG-rich nanoclusters that promote fast ion transport across the organic|aqueous interface, yielding a wide ESW (0.0–4.9 V versus Li|Li^+) and sustained capacity retention over 80 cycles in a lithium metal pouch cell[131].

A step further is the complete elimination of a solvent, relying solely on salt mixtures as the liquid electrolyte formulation. In 2023, Vu et al. reported a solvent-free inorganic molten salt mixture composed of alkali-based bis(fluorosulfonyl)amide salts, combining the non-volatility and safety features of solids with the interfacial stability and high ionic conductivity of organic liquids[132]. Binary ($Li_{0.45}K_{0.55}FSI$) and ternary ($Li_{0.30}K_{0.35}Cs_{0.35}FSI$) salts melt at 68 °C and 45 °C, respectively, with ~1 mS cm^{-1} conductivity at 60 °C and very high oxidative stability up to 6 V versus Li|Li^+. These molten salts enable compact Li deposition, inorganic SEI formation, high average CEs (up to 99.8%) and low overpotentials (50 mV at 5 mA cm^{-2}) at 80 °C (Fig. 4)[132].

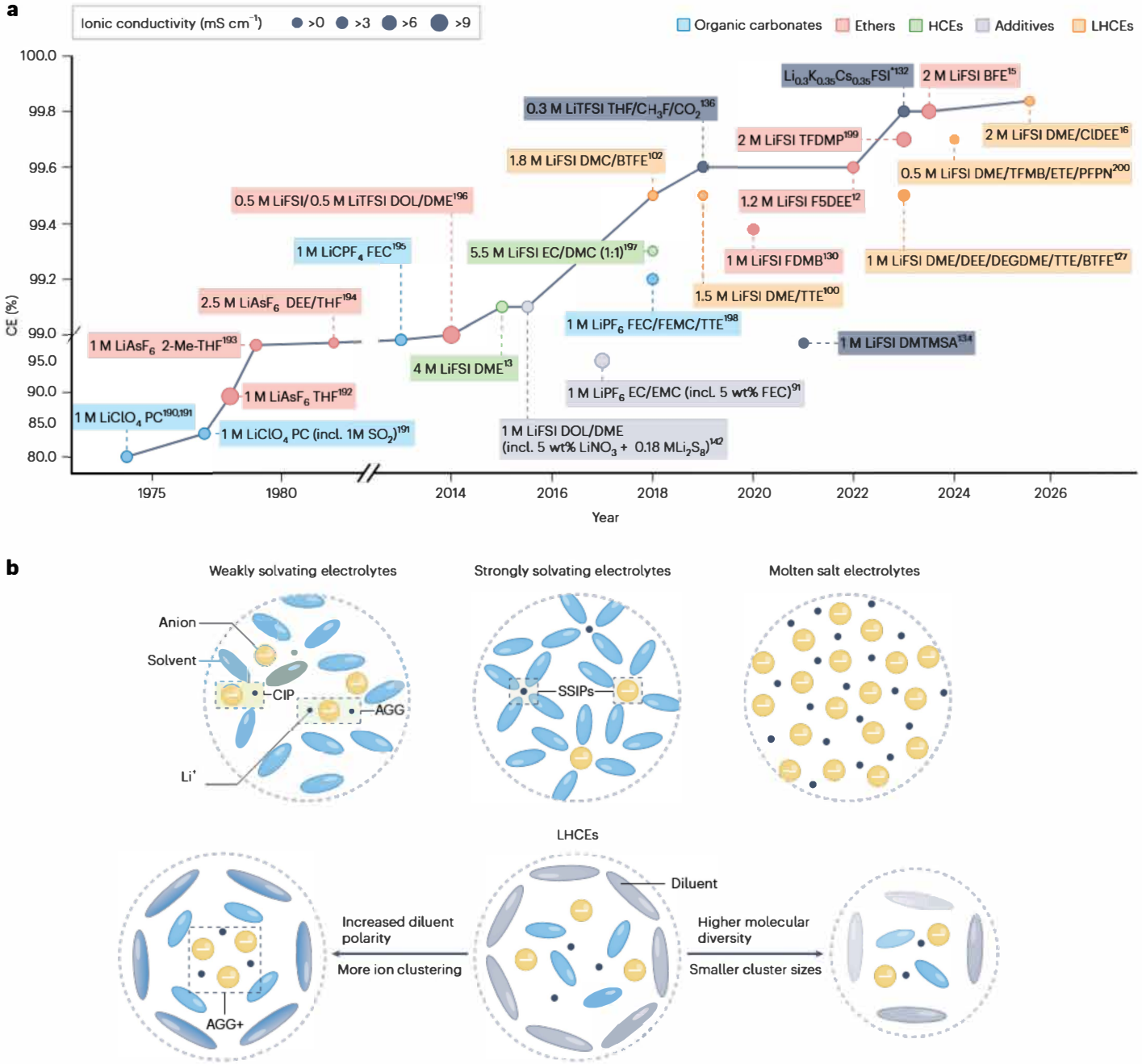

Fig. 4 | Historical evolution of electrolyte concepts to enable efficient Li stripping/plating. a, Evolution of the composition of the liquid electrolyte solutions and performance assessment of the cells' Li stripping/plating efficiency (i.e., CE). The CE values reported in the graph are calculated from the galvanostatic cycling of Li||Cu coin cells at current densities of at least 0.5 mA cm^{-2}. The presented experimental data are determined between 20 and 25 °C, while data marked with an asterisk are collected at 80 °C. The salt concentration (M) was unified as moles per litre of electrolyte. DEE, 1,2-diethoxyethane; FEC, fluoroethylene carbonate; DOL, 1,3-dioxolane; DMC, dimethyl carbonate; FDMB, 2,2,3,3-tetrafluoro-1,4-dimethoxylbutane; FSDEE, 2-[2-(2,2-difluoroethoxy)ethoxy]-1,1,1-trifluoroethane; DEGDME, 2-methoxyethyl ether; TFMB, trifluoromethoxy-benzene; ETE, ethyl 1,1,2,2-tetrafluoroethyl ether; PFPN, ethoxy(pentafluoro)cyclotriphosphazene; PC, propylene carbonate; THF, tetrahydrofuran; 2-Me-THF, 2-methyltetrahydrofuran; EMC, ethyl methyl carbonate; FEMC, methyl (2,2,2-trifluoroethyl) carbonate; BTFE, bis(2,2,2-trifluorethyl)ether[108,136,190–200]. **b**, Schematic representation of selected solvation structures of liquid electrolyte solutions for LMBs, including weakly solvating solvent electrolytes with an increased interaction between the ions, molten salt electrolytes with no solvent present and LHCEs. SSIPs, solvent-separated ion pairs. Panel a adapted from ref. 1, Springer Nature Limited.

Strongly solvating electrolytes

Although weakly coordinating electrolytes have attracted substantial attention in recent years due to their effective anion-derived SEI formation, several strongly solvating solvents have been identified to facilitate efficient Li stripping/plating (Fig. 4b).

In 2020, Xue et al. introduced the concept of full fluorosulfonyl electrolytes by coupling LiFSI with an FSI-derived solvent, DMTMSA ($FSO_2NC_2H_6$)[133,134]. This electrolyte formulation promotes the formation of a highly robust LiF-enriched SEI, achieving an initial cell CE of 91%, which rapidly increases to 99% within ten cycles (Fig. 4a). The high compatibility of full fluorosulfonyl electrolytes with the lithium metal electrode can be attributed to the physicochemical properties of the solvent. DFT calculations and experimental analyses indicate that full fluorosulfonyl solvents have a higher binding energy with Li^+

than fluoroethylene carbonate, promoting release of the fluorine group and formation of a solvent and anion-derived inorganic-rich SEI that effectively suppresses dendritic growth and enhances the overall stability of the interphase layer SEI.

Fluoro- and difluoro-methane are used as electrolyte solvents in pressure-controlled batteries, achieving high average cell CEs of up to 99.6% and showing promising results across a wide temperature range of −60 to 60 °C (Fig. 4a)[135,136].

Multisalt electrolytes and film-forming additives

Several salt combinations and film-forming (i.e., SEI) additives have been explored to enhance the electrochemical performance of LMBs (Fig. 4a). Researchers utilize lithium difluoro(oxalate)borate[137,138], $LiNO_3$[139–142] and various sulfonyl imides[139,140,143] in multiple blended salt electrolytes, showing synergistic effects during SEI formation. However, LiFSI remains the most promising salt for LMB electrolyte solutions due to its well-rounded properties and effective film-forming abilities. Among the many additives proposed for LMB electrolyte solutions, fluorination agents (such as FEC[91,144] and difluoroethylene carbonate[145]) and $LiNO_3$[139–141] proved to be highly effective in promoting a beneficial SEI composition and compact Li deposition. However, continuous SEI reformation/repair in the negative electrode of the LMB during galvanostatic cycling rapidly consumes film-forming additives, reducing their effectiveness after a few cycles[144]. In contrast, Ding et al.[146] reported Cs-based salts as non-sacrificial additives that promote homogeneous and compact Li deposition morphologies due to an electrostatic shield mechanism induced by Cs^+ ions[144,147].

In summary, various electrolyte solution designs with nanoengineering aspects show promise at a low technology readiness level (TRL) towards future commercialization of LMBs[148]. In particular, LHCEs and fluorinated ether electrolytes stand out for their cell performance, cost-effectiveness and manufacturing compatibility. Molten salt and liquefied gas electrolytes also provide excellent low-TRL cell cycling performance due to the formation of a robust inorganic-rich SEI. However, these two types of electrolyte are limited by more stringent galvanostatic cycling conditions and higher costs, probably confining them to niche applications.

Analytical techniques

Various basic and advanced techniques and methods are used to evaluate the key properties of nanoengineered LMB electrolyte solutions against current state-of-the-art electrolytes. These are summarized in Table 1.

To assess the performance of LMB electrolyte solutions, it is essential to design a laboratory-scale experiment that takes into account the cell's parameters and evaluation conditions identified as standard by the international battery research community. The most important parameters are reported in Table 2.

Electrochemical techniques

The so-called 'Aurbach method', generally carried out in a Li‖Cu laboratory-scale cell configuration (usually a coin cell), is the standard electrochemical method for determining CE and Li loss per cycle, while long-term cycling gives valuable information about CE evolution during the cell's cycling life[149]. Since Li stripping/plating efficiency is a crucial parameter for LMB performance, understanding of the CE values, calculated using the Aurbach method, is essential for evaluating the ability of an electrolyte solution to form an effective lithium passivation layer (an SEI) and improve the cell's cycle life.

Information about the internal cell resistances can be obtained by analysing the cell's potential profile evolution and conducting electrochemical impedance spectroscopy measurements. Indeed, through the analysis of raw electrochemical impedance spectroscopy data, the various resistance contributions (e.g., associated with the electrolyte solution, electrodes' interface or electrode|electrolyte interphases) can be identified via equivalent circuit or physics-based modelling[150–152]. In terms of data analysis, the use of dQ/dV and dV/dQ plots, derived from potential and capacity data, provides valuable insights into the degradation processes taking place in LMBs: e.g., loss of Li inventory and increase of the cell's impedance during galvanostatic cycling. This type of electrochemical measurement also offers valuable insights for the design of advanced post mortem or in situ measurements[153].

Table 1 | Examples of techniques and methods used to investigate the physicochemical and electrochemical properties of non-aqueous electrolyte solutions for LMBs

Property	Technique/method	Set-up/tools
Solvation structure	Raman spectroscopy[201]	Raman spectrometer and sample carrier for liquids
	X-ray scattering[127,202]	Electrolyte sample placed between X-ray beam and detector
	Molecular dynamics simulations[127]	Theoretical simulation based on calculated quantum data (i.e., DFT)
Ion mobility	Electrochemical impedance spectroscopy[150]	Commercially available ionic conductivity cells/sensors
	Pulsed-field gradient NMR[203], electrophoretic NMR[26,203], Hittorf measurements[23,24]	Experimental set-ups adjusted to a specific method
ESW	Linear sweep voltammetry, cyclic voltammetry[204]	Three-electrode laboratory-scale cell configurations (e.g., Swagelok or El-cell)
Flammability	Self-extinguishing time determination[205]	Non-flammable electrolyte-containing porous material (e.g., glass fibre separator membrane) and ignition source
	Flash point determination[205]	Temperature-controlled electrolyte container and ignition source
Thermal stability	Differential scanning calorimetry[206]	Differential scanning calorimetry device, electrolyte sample and reference
	Thermogravimetric analysis[207]	Thermogravimetric analysis device and electrolyte sample

Interface and interphase characterizations

Characterizations of the electrode interface and electrode|electrolyte interphases are challenging and require approaches that allow measurements under in situ (i.e., the characterization is carried out while the electrochemical measurement is paused) or operando (i.e., the characterization is carried out while the electrochemical measurement is running) conditions to mimic practical cell operation conditions[154]. Macroscopic electrochemical techniques assess overall performance at TRLs ≥ 4 (ref. 148), whereas analytical techniques operating at the micro- and nanoscale at molecular and elemental levels reveal interphase structure and chemistry. This integrated approach could lead to the design of tailored interphases, bridging laboratory-scale research and practical applications, thus advancing scientific progress towards high TRLs (Fig. 5)[148,155].

Microscopic insights

The nanoscale structure of the SEI requires advanced analytical techniques with high spatial resolution. Scanning electron microscopy (SEM), a powerful tool for investigating the Li deposition morphology, can provide detailed two-/three-dimensional microstructural information, ranging from micrometre to nanometre scale. Cryogenic TEM measurements are also effective in revealing the structural properties of the SEI layer, owing to the very high spatial resolution (down to the atomic scale) and reduced beam damage[42,156]. This approach assisted in elucidating the SEI nanostructure[42,156], the effect of the current density on the SEI evolution[88], the relationship

Table 2 | Essential cell parameters and evaluation conditions to assess the performance of LMB electrolyte solutions

	Negative electrode	Positive electrode	Separator and electrolyte amount	Galvanostatic cycling conditions
Requirement	Limited Li reservoir (<50 µm)	State-of-the-art materials with high loadings (>3 mAh cm^{-2})	Thin separator (~20 µm) with limited electrolyte quantity (~2–3 g Ah^{-1})	Application-oriented multilayer cell format (e.g., >100 mAh), current density (>1.0 mA cm^{-2}) and cutoff potential (vs Li|Li$^+$, depending on cell chemistry)

between the SEI and the Li morphology[157], the link between cell performance and operating temperature[66] and the correlation between SEI composition and the cell's CEs[96,130]. Moreover, the combination of two-dimensional space images with two-dimensional diffraction pattern four-dimensional-scanning TEM measurements enables the simultaneous identification of the SEI's nanoscale crystallinity and composition, as well as visualization of the strain and electric fields of the SEI via differential phase-contrast or centre-of-mass imaging[85,158]. While most EM experiments are conducted ex situ, necessitating sample preparation, which might alter the interphase properties, developed in situ set-ups allow microscopic investigations during cell operation[159]. Another technique often applied to study the morphology and mechanical properties of the SEI and Li deposits is electrochemical atomic force microscopy (EC-AFM); its in situ capability makes it a powerful tool for fundamental research[160,161].

Identification, quantification and distribution of chemical species in the SEI

A wide range of analytical techniques is required to identify and quantify the inorganic and organic compounds in the SEI (Fig. 5). However, the difficulty of analysis depends on the compound. Common identification of most inorganic compounds can be achieved by analysing the electrodes via ex situ X-ray photoelectron spectroscopy (XPS)[54], X-ray diffraction[162], time-of-flight SIMS (ToF-SIMS)[163], Fourier transform infrared (FTIR)[164], Raman spectroscopy[165] or NMR spectroscopy[166] measurements. In particular, ToF-SIMS, FTIR, Raman and NMR provide information on both inorganic and organic compounds. ^{7}Li NMR is also a powerful technique for analysing morphological changes in the Li metal electrode and quantifying the formation of dead Li even in situ[167].

As the identification and quantification of organic SEI compounds is more challenging than that of inorganic species, researchers reported the detection of functional groups or repetitive structural motifs, such as $-CO_3$, C–O, C=O or C–H by ex or in situ electrode analysis via XPS[54] or FTIR[164] measurements. These techniques are, however, limited in identifying or reconstructing entire molecular structures in the SEI, necessitating mass spectrometry to identify and characterize more complex organic compounds (e.g., oligomers)[163].

By combining microscopic (e.g., SEM, TEM) and spectroscopic (e. g., FTIR, Raman) techniques, it becomes possible to simultaneously obtain spatial and chemical information about formed interphases. Energy dispersive spectroscopy (EDS) detectors are often integrated into SEMs, yielding information about the spatial elemental distribution[168]. Cryogenic scanning TEM has also been successfully paired with electron energy loss spectroscopy and EDS to obtain high-resolution structural and chemical information as well as to characterize electronic structures and bonding environments[169]. In addition to electron microscopy techniques, AFM can be combined with IR spectroscopy to couple the morphological and mechanical information gained by AFM with chemical information about the interphase[170].

Finally, multiscale modelling based on first-principle methods, such as DFT and ab initio molecular dynamics, can provide a deeper understanding of interphase formation processes and decomposition reaction pathways[171,172]. Less computationally expensive ab initio-based mesoscale techniques (i.e., kinetic Monte Carlo) can capture the interphase dynamics over larger timescales (up to hours) and enable a direct correlation with experimental data[93,173]. To advance the understanding of the SEI and its complex nature, the combined use of complementary experimental and theoretical techniques is necessary to correlate structural and chemical information with other interphase layer properties. Further refinement and development of novel in situ and operando techniques with short measurement times allows the study of dynamic electrochemical processes, bridging the gap between experimental data and simulations.

Conclusion and perspective

Advanced nanoengineering design of electrolyte solutions enables electrochemical performance improvements of laboratory-scale LMBs (i.e., with TRLs < 4). However, to develop practical zero-excess LMBs at TRL ≥ 4 with a cycle life comparable to that of current commercial LIBs, the average CE must be in the 99.95–99.98% range (80% state of health after 450–1,100 cycles). To achieve this goal, addressing the challenges of producing an effective Li metal electrode protection interlayer (i.e., the SEI) that enables minimal losses of active material during galvanostatic cycling is crucial. State-of-the-art research suggests aiming for fast SEI formation kinetics with homogeneously distributed inorganic-rich decomposition products such as Li_3N, Li_2O and LiF due to their high mechanical strength combined with good electronic insulating properties to promote a compact Li deposition morphology. The presence of organic polymeric species in the SEI's outer layer is also considered beneficial, increasing the flexibility and adaptability of the interphase layer to the mechanical stress during Li plating/stripping. Due to the SEI's brittle and air/moisture-sensitive nature, complementary in situ and operando analysis techniques are required to investigate relevant formation processes and interphase properties. Increasing the measurements' temporal resolution is also crucial to capture the short-lived intermediate species and fast SEI evolution mechanisms, as well as closing the gap with theoretical simulations, usually operating in narrow time frames.

Furthermore, to enable prolonged and effective cell performance, it is necessary for electrolyte solutions to guarantee a preferential rapid reductive decomposition of the salt-derived anion by simultaneously achieving sufficient oxidative stability as well as a high ionic conductivity (>3 mS cm^{-1} at ~1 M salt concentration at 20–25 °C) to avoid dendrite formation and ensure compact Li deposition at high currents. The development of a nanoengineering approach to understand the Li^+ ion solvation sheath, including the size and shape of the resulting clusters and the binding strength between each pair of electrolyte components, is crucial for producing electrolyte solutions with tailored electrochemical and physicochemical properties. Simultaneously, industry-relevant electrolyte features such as costs, safety, environmental impact and operational temperatures should be considered to determine if an electrolyte formulation can transition from low to high TRLs[174].

Researchers have explored various approaches to meet the challenging requirements for achieving high cell CEs under practical conditions. One of these approaches focuses on the design of electrolyte components, especially solvents, which can help tune the solvation sheath to improve the electrolyte properties and favour the formation of a more effective SEI. Starting from simple mono- and diether molecules, rational and systematic synthesis of derivatives with electron-withdrawing or sterically demanding groups has already been shown to yield solvents that enable very efficient Li plating/stripping. Systematic study of ether backbone structure and functional group position guides synthesis to optimize Li^+ ion solvation strength

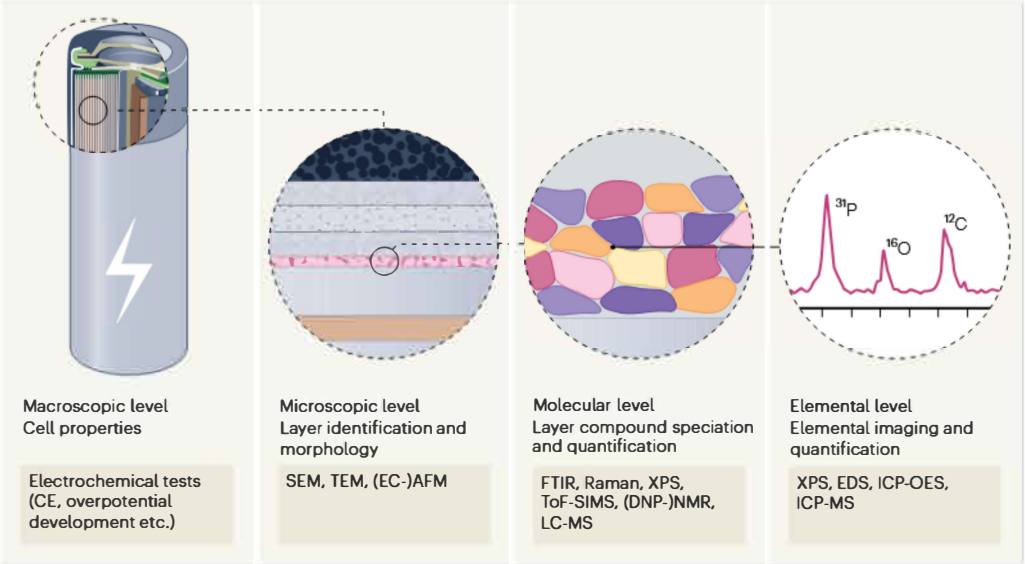

Fig. 5 | Characterization techniques for LMBs. Overview of the characterization techniques, ranging from the macroscopic cell level to the elemental level, used to study the interfaces and interphases in batteries. DNP, dynamic nuclear polarization; LC, liquid chromatography; MS, mass spectrometry; ICP, inductive coupled plasma; OES, optical emission spectrometry.

and clusters. A deeper understanding of solvent–diluent interactions in LHCEs is also needed to link solvation dynamics with interphase formation and ionic conductivity. Tailored diluents and high-entropy designs enable simultaneous optimization of solvation strength and ion mobility. While liquefied gas and molten salt electrolytes enhance Li metal passivation, their galvanostatic cycling constraints and costs limit widespread use. Establishing structure–property relationships between Li salts and the SEI supports rational anion design, with salt–solvent combinations in LHCEs fine-tuning solvation. Adequate functional additives may further improve the cell's performance but require detailed knowledge of their interactions, effects and consumption during galvanostatic cycling.

The vast chemical space and modern synthesis offer substantial opportunities for designing application-tailored electrolytes; however, the complexity and time required for complete characterization make preselection and rapid screening essential to identify promising candidates. Here, three methods are gaining increasingly more attention: (1) high-throughput experimentation[175], which accelerates the experimental screening of promising electrolyte compositions, (2) high-throughput quantum mechanical calculations, which calculate electrolyte properties or substitute for time-intensive experiments, and (3) machine learning (ML), which enables predictions of electrolyte components/compositions based on an extensive database of internal (generally confidential) and public experimental and simulation data. ML enables exploration of vast chemical space by correlating molecular structures with intrinsic electrolyte properties and performance data, thereby identifying the key property-based descriptors that most strongly influence targeted performance metrics[176,177]. The screening scope spans all potential liquid electrolyte solution molecules, estimated to be between 10^9 and 10^{10} candidates.

Current ML models typically predict electrolyte properties from known parameters, whereas an attribute-driven inverse design approach, using target performance metrics to identify candidate electrolytes, is favoured for rational electrolyte development (Fig. 6)[178]. Identifying improved structural descriptors for target properties is crucial to efficiently screen the vast space of possible electrolyte compositions. Subsequent high-throughput quantum mechanical calculations can prescreen the components proposed by ML algorithms[179,180]. Quantum mechanical data from the most promising candidates further support advanced simulations, estimating bulk and dynamic properties, and providing insights into SEI formation via ab initio methods[179]. After targeted synthesis and formulation of the most promising electrolyte candidates, high-throughput experimentation can be utilized to acquire desired datasets[181,182]. When coupled with ML analysis, high-throughput experimentation enables optimization of bulk ionic conductivity and identification of the optimum electrolyte compositions[181–183]. Continuous refinement of ML models, acquired datasets, standardized experimental protocols and open-source databases across institutions will further improve electrolyte formulation predictions, accelerated by advanced simulations and AI-powered computing.

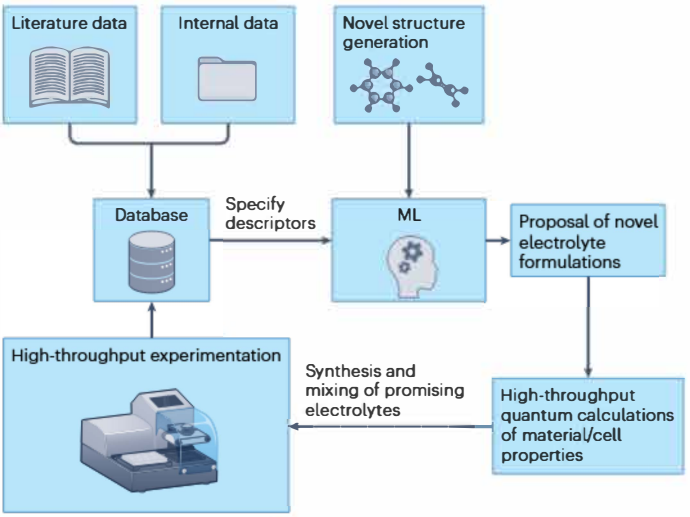

Fig. 6 | Iterative process for accelerated electrolyte development. An iterative process scheme for accelerated electrolyte development incorporating advanced ML and high-throughput calculations and experimentation. DFT calculations can be utilized to explore novel component structures from the vast scope of potential molecules (up to 10^{10} candidates).

In summary, the development of non-aqueous electrolytes for LMBs demands a holistic approach balancing materials, manufacturing and safety to achieve high-performance and cost-effective solutions suitable for practical applications.

References

1. Hobold, G. M. et al. Moving beyond 99.9% Coulombic efficiency for lithium anodes in liquid electrolytes. *Nat. Energy* **6**, 951–960 (2021).
2. Horstmann, B. et al. Strategies towards enabling lithium metal in batteries: interphases and electrodes. *Energy Environ. Sci.* **14**, 5289–5314 (2021).
3. Brandt, K. & Laman, F. C. Reproducibility and reliability of rechargeable lithium/molybdenum disulfide batteries. *J. Power Sources* **25**, 265–276 (1989).
4. Fang, C., Wang, X. & Meng, Y. S. Key issues hindering a practical lithium-metal anode. *Trends Chem.* **1**, 152–158 (2019).
5. Liu, J. et al. Pathways for practical high-energy long-cycling lithium metal batteries. *Nat. Energy* **4**, 180–186 (2019).
6. Jagger, B. & Pasta, M. Solid electrolyte interphases in lithium metal batteries. *Joule* **7**, 2228–2244 (2023).
7. He, X. et al. The passivity of lithium electrodes in liquid electrolytes for secondary batteries. *Nat. Rev. Mater.* **6**, 1036–1052 (2021).
8. Lu, D. et al. Failure mechanism for fast-charged lithium metal batteries with liquid electrolytes. *Adv. Energy Mater.* **5**, 1400993 (2015).
9. Wang, H. et al. Liquid electrolyte: the nexus of practical lithium metal batteries. *Joule* **6**, 588–616 (2022).
10. Boyle, D. T. et al. Correlating kinetics to cyclability reveals thermodynamic origin of lithium anode morphology in liquid electrolytes. *J. Am. Chem. Soc.* **144**, 20717–20725 (2022).
11. Giffin, G. A. The role of concentration in electrolyte solutions for non-aqueous lithium-based batteries. *Nat. Commun.* **13**, 5250 (2022).
12. Yu, Z. et al. Rational solvent molecule tuning for high-performance lithium metal battery electrolytes. *Nat. Energy* **7**, 94–106 (2022).
    Systematic design of bi-ethers to optimize the thermodynamic and kinetic properties of liquid electrolytes.
13. Qian, J. et al. High rate and stable cycling of lithium metal anode. *Nat. Commun.* **6**, 6362 (2015).
14. Choi, I. R. et al. Asymmetric ether solvents for high-rate lithium metal batteries. *Nat. Energy* **10**, 365–379 (2025).
15. Zhang, G. et al. A monofluoride ether-based electrolyte solution for fast-charging and low-temperature non-aqueous lithium metal batteries. *Nat. Commun.* **14**, 1081 (2023).
    Single-solvent mono-ether-based electrolyte enabling efficient Li stripping/plating at high current densities.
16. Yang, W., Chen, A., He, P. & Zhou, H. Advancing lithium metal electrode beyond 99.9% coulombic efficiency via super-saturated electrolyte with compressed solvation structure. *Nat. Commun.* **16**, 4229 (2025).
17. Xu, K. *Electrolytes, Interfaces and Interphases* (Royal Society of Chemistry, 2023).
18. Zhou, P., Xiang, Y. & Liu, K. Understanding and applying the donor number of electrolytes in lithium metal batteries. *Energy Environ. Sci.* **17**, 8057–8077 (2024).
19. Goodenough, J. B. & Kim, Y. Challenges for rechargeable Li batteries. *Chem. Mater.* **22**, 587–603 (2010).
20. Peljo, P. & Girault, H. H. Electrochemical potential window of battery electrolytes: the HOMO–LUMO misconception. *Energy Environ. Mater.* **11**, 2306–2309 (2018).
21. Xu, K., Ding, S. P. & Jow, T. R. Toward reliable values of electrochemical stability limits for electrolytes. *J. Electrochem. Soc.* **146**, 4172–4178 (1999).
22. Sethurajan, A. K., Krachkovskiy, S. A., Halalay, I. C., Goward, G. R. & Protas, B. Accurate characterization of ion transport properties in binary symmetric electrolytes using in situ NMR imaging and inverse modeling. *J. Phys. Chem. B* **119**, 12238–12248 (2015).
23. Hou, T. & Monroe, C. W. Composition-dependent thermodynamic and mass-transport characterization of lithium hexafluorophosphate in propylene carbonate. *Electrochim. Acta* **332**, 135085 (2020).
24. Wang, A. A., Hou, T., Karanjavala, M. & Monroe, C. W. Shifting-reference concentration cells to refine composition-dependent transport characterization of binary lithium-ion electrolytes. *Electrochim. Acta* **358**, 136688 (2020).
25. Diederichsen, K. M., McShane, E. J. & McCloskey, B. D. Promising routes to a high Li^+ transference number electrolyte for lithium ion batteries. *ACS Energy Lett.* **2**, 2563–2575 (2017).
26. Lorenz, M. et al. Local volume conservation in concentrated electrolytes is governing charge transport in electric fields. *J. Phys. Chem. Lett.* **13**, 8761–8767 (2022).
27. Schammer, M., Horstmann, B. & Latz, A. Theory of transport in highly concentrated electrolytes. *J. Electrochem. Soc.* **168**, 026511 (2021).
28. Zugmann, S. et al. Measurement of transference numbers for lithium ion electrolytes via four different methods, a comparative study. *Electrochim. Acta* **56**, 3926–3933 (2011).
29. Petrowsky, M., Frech, R., Suarez, S. N., Jayakody, J. R. P. & Greenbaum, S. Investigation of fundamental transport properties and thermodynamics in diglyme–salt solutions. *J. Phys. Chem. B* **110**, 23012–23021 (2006).
30. Kwabi, D. G. et al. Experimental and computational analysis of the solvent-dependent $O_2/Li^+–O_2^-$ redox couple: standard potentials, coupling strength, and implications for lithium–oxygen batteries. *Angew. Chem. Int. Ed.* **55**, 3129–3134 (2016).
31. Leverick, G. & Shao-Horn, Y. Controlling electrolyte properties and redox reactions using solvation and implications in battery functions: a mini-review. *Adv. Energy Mater.* **13**, 2204094 (2023).
32. Ko, S. et al. Electrode potential influences the reversibility of lithium-metal anodes. *Nat. Energy* **7**, 1217–1224 (2022).
33. Wu, Q., McDowell, M. T. & Qi, Y. Effect of the electric double layer (EDL) in multicomponent electrolyte reduction and solid electrolyte interphase (SEI) formation in lithium batteries. *J. Am. Chem. Soc.* **145**, 2473–2484 (2023).
34. Angarita-Gomez, S. & Balbuena, P. B. Solvation *vs*. surface charge transfer: an interfacial chemistry game drives cation motion. *Chem. Commun.* **57**, 6189–6192 (2021).
35. Xu, K. Electrolytes and interphases in Li-ion batteries and beyond. *Chem. Rev.* **114**, 11503–11618 (2014).
36. Camacho-Forero, L. E., Smith, T. W. & Balbuena, P. B. Effects of high and low salt concentration in electrolytes at lithium-metal anode surfaces. *J. Phys. Chem. C* **121**, 182–194 (2017).
37. Sayah, S. et al. How do super concentrated electrolytes push the Li-ion batteries and supercapacitors beyond their thermodynamic and electrochemical limits?. *Nano Energy* **98**, 107336 (2022).
38. Dokko, K. et al. Direct evidence for Li ion hopping conduction in highly concentrated sulfolane-based liquid electrolytes. *J. Phys. Chem. B* **122**, 10736–10745 (2018).
39. Raccichini, R., Dibden, J. W., Brew, A., Owen, J. R. & García-Aráez, N. Ion speciation and transport properties of LiTFSI in 1,3-dioxolane solutions: a case study for Li–S battery applications. *J. Phys. Chem. B* **122**, 267–274 (2018).
40. Chen, Y. et al. Steric effect tuned ion solvation enabling stable cycling of high-voltage lithium metal battery. *J. Am. Chem. Soc.* **143**, 18703–18713 (2021).
41. Lin, Y.-X. et al. Connecting the irreversible capacity loss in Li-ion batteries with the electronic insulating properties of solid electrolyte interphase (SEI) components. *J. Power Sources* **309**, 221–230 (2016).
42. Li, Y. et al. Atomic structure of sensitive battery materials and interfaces revealed by cryo-electron microscopy. *Science* **358**, 506–510 (2017).
43. Wang, M. et al. Effect of LiFSI concentrations to form thickness- and modulus-controlled SEI layers on lithium metal anodes. *J. Phys. Chem. C* **122**, 9825–9834 (2018).

44. Zhang, Z. et al. Capturing the swelling of solid-electrolyte interphase in lithium metal batteries. *Science* **375**, 66–70 (2022).
45. Li, Y. & Qi, Y. Transferable self-consistent charge density functional tight-binding parameters for Li-metal and Li-ions in inorganic compounds and organic solvents. *J. Phys. Chem. C* **122**, 10755–10764 (2018).
46. Soto, F. A., Ma, Y., Martinez De La Hoz, J. M., Seminario, J. M. & Balbuena, P. B. Formation and growth mechanisms of solid–electrolyte interphase layers in rechargeable batteries. *Chem. Mater.* **27**, 7990–8000 (2015).
47. Single, F., Latz, A. & Horstmann, B. Identifying the mechanism of continued growth of the solid-electrolyte interphase. *ChemSusChem* **11**, 1950–1955 (2018).
48. Von Kolzenberg, L., Latz, A. & Horstmann, B. Solid–electrolyte interphase during battery cycling: theory of growth regimes. *ChemSusChem* **13**, 3901–3910 (2020).
49. Single, F., Horstmann, B. & Latz, A. Dynamics and morphology of solid electrolyte interphase (SEI). *Phys. Chem. Chem. Phys.* **18**, 17810–17814 (2016).
50. Single, F., Horstmann, B. & Latz, A. Revealing SEI morphology: in-depth analysis of a modeling approach. *J. Electrochem. Soc.* **164**, E3132–E3145 (2017).
51. Harris, O. C., Lin, Y., Qi, Y., Leung, K. & Tang, M. H. How transition metals enable electron transfer through the SEI: part I. Experiments and Butler–Volmer modeling. *J. Electrochem. Soc.* **167**, 013502 (2020).
52. Menkin, S. et al. Toward an understanding of SEI formation and lithium plating on copper in anode-free batteries. *J. Phys. Chem. C* **125**, 16719–16732 (2021).
53. Wang, H. et al. The effect of removing the native passivation film on the electrochemical performance of lithium metal electrodes. *J. Power Sources* **520**, 230817 (2022).
54. Kühn, S. P. et al. Back to the basics: advanced understanding of the as-defined solid electrolyte interphase on lithium metal electrodes. *J. Power Sources* **549**, 232118 (2022).
55. Otto, S.-K. et al. Storage of lithium metal: the role of the native passivation layer for the anode interface resistance in solid state batteries. *ACS Appl. Energy Mater.* **4**, 12798–12807 (2021).
56. Yoon, J. S. et al. Thermodynamics, adhesion, and wetting at Li/Cu(-oxide) interfaces: relevance for anode-free lithium-metal batteries. *ACS Appl. Mater. Interfaces* **16**, 18790–18799 (2024).
57. Aravindan, V., Gnanaraj, J., Madhavi, S. & Liu, H. Lithium-ion conducting electrolyte salts for lithium batteries. *Chem. Eur. J.* **17**, 14326–14346 (2011).
58. Schmitz, R. W. et al. Investigations on novel electrolytes, solvents and SEI additives for use in lithium-ion batteries: systematic electrochemical characterization and detailed analysis by spectroscopic methods. *Prog. Solid State Chem.* **42**, 65–84 (2014).
59. Yeddala, M., Rynearson, L. & Lucht, B. L. Modification of carbonate electrolytes for lithium metal electrodes. *ACS Energy Lett.* **8**, 4782–4793 (2023).
60. Bai, P., Li, J., Brushett, F. R. & Bazant, M. Z. Transition of lithium growth mechanisms in liquid electrolytes. *Energy Environ. Sci.* **9**, 3221–3229 (2016).
61. Shin, W. & Manthiram, A. A facile potential hold method for fostering an inorganic solid-electrolyte interphase for anode-free lithium-metal batteries. *Angew. Chem.* **134**, e202115909 (2022).
62. Kwon, Y. et al. Elucidating the role of cathode identity: voltage-dependent reversibility of anode-free batteries. *Chem* **10**, 3159–3183 (2024).
63. Fang, C. et al. Pressure-tailored lithium deposition and dissolution in lithium metal batteries. *Nat. Energy* **6**, 987–994 (2021).
64. Lei, Y. et al. Recent advances in separator design for lithium metal batteries without dendrite formation: implications for electric vehicles. *eTransportation* **20**, 100330 (2024).
65. Ishikawa, M., Tasaka, Y., Yoshimoto, N. & Morita, M. Optimization of physicochemical characteristics of a lithium anode interface for high-efficiency cycling: an effect of electrolyte temperature. *J. Power Sources* **97/98**, 262–264 (2001).
66. Wang, J. et al. Improving cyclability of Li metal batteries at elevated temperatures and its origin revealed by cryo-electron microscopy. *Nat. Energy* **4**, 664–670 (2019).
67. Sheng, S., Sheng, L., Wang, L., Piao, N. & He, X. Thickness variation of lithium metal anode with cycling. *J. Power Sources* **476**, 228749 (2020).
68. McBrayer, J. D., Apblett, C. A., Harrison, K. L., Fenton, K. R. & Minteer, S. D. Mechanical studies of the solid electrolyte interphase on anodes in lithium and lithium ion batteries. *Nanotechnology* **32**, 502005 (2021).
69. Yuan, S. et al. Revisiting the designing criteria of advanced solid electrolyte interphase on lithium metal anode under practical condition. *Nano Energy* **83**, 105847 (2021).
70. Shen, X. et al. The failure of solid electrolyte interphase on Li metal anode: structural uniformity or mechanical strength? *Adv. Energy Mater.* **10**, 1903645 (2020).
71. Werres, M. et al. Origin of heterogeneous stripping of lithium in liquid electrolytes. *ACS Nano* **17**, 10218–10228 (2023).
72. Gao, Y. et al. Unraveling the mechanical origin of stable solid electrolyte interphase. *Joule* **5**, 1860–1872 (2021).
73. Gu, Y. et al. Designable ultra-smooth ultra-thin solid-electrolyte interphases of three alkali metal anodes. *Nat. Commun.* **9**, 1339 (2018).
74. Wang, J. et al. In situ self-assembly of ordered organic/inorganic dual-layered interphase for achieving long-life dendrite-free Li metal anodes in LiFSI-based electrolyte. *Adv. Funct. Mater.* **31**, 2007434 (2021).
75. Xu, Y. et al. Theoretical calculation study on the electrochemical properties of lithium halide-based artificial SEI films for lithium metal anodes. *Surf. Interfaces* **44**, 103768 (2024).
76. Shi, S. et al. Direct calculation of Li-ion transport in the solid electrolyte interphase. *J. Am. Chem. Soc.* **134**, 15476–15487 (2012).
77. Lu, P. & Harris, S. J. Lithium transport within the solid electrolyte interphase. *Electrochem. Commun.* **13**, 1035–1037 (2011).
Investigation of Li^+ transport in the SEI via isotope exchange experiments.
78. Yu, X. et al. Direct and in situ examination of Li^+ transport kinetics in an isotope-labeled solid–electrolyte interphase. *Proc. Natl Acad. Sci. USA* **122**, e2514652122 (2025).
79. Das Goswami, B. R., Jabbari, V., Shahbazian-Yassar, R., Mashayek, F. & Yurkiv, V. Unraveling ion diffusion pathways and energetics in polycrystalline SEI of lithium-based batteries: combined cryo-HRTEM and DFT study. *J. Phys. Chem. C* **127**, 21971–21979 (2023).
80. Soto, F. A., Marzouk, A., El-Mellouhi, F. & Balbuena, P. B. Understanding ionic diffusion through SEI components for lithium-ion and sodium-ion batteries: insights from first-principles calculations. *Chem. Mater.* **30**, 3315–3322 (2018).
81. Xu, Y. et al. Direct in situ measurements of electrical properties of solid-electrolyte interphase on lithium metal anodes. *Nat. Energy* **8**, 1345–1354 (2023).
Experimental evidence of the electrical semiconducting properties of the SEI.
82. Benitez, L. & Seminario, J. M. Electron transport and electrolyte reduction in the solid-electrolyte interphase of rechargeable lithium ion batteries with silicon anodes. *J. Phys. Chem. C* **120**, 17978–17988 (2016).

83. Derosa, P. A. & Seminario, J. M. Electron transport through single molecules: scattering treatment using density functional and Green function theories. *J. Phys. Chem. B* **105**, 471–481 (2001).
84. Köbbing, L., Latz, A. & Horstmann, B. Growth of the solid-electrolyte interphase: electron diffusion versus solvent diffusion. *J. Power Sources* **561**, 232651 (2023).
85. Feng, M., Pan, J. & Qi, Y. Impact of electronic properties of grain boundaries on the solid electrolyte interphases (SEIs) in Li-ion batteries. *J. Phys. Chem. C* **125**, 15821–15829 (2021).
86. Fang, C. et al. Quantifying inactive lithium in lithium metal batteries. *Nature* **572**, 511–515 (2019).
87. Steiger, J., Kramer, D. & Mönig, R. Mechanisms of dendritic growth investigated by in situ light microscopy during electrodeposition and dissolution of lithium. *J. Power Sources* **261**, 112–119 (2014).
88. Xu, Y. et al. Current density regulated atomic to nanoscale process on Li deposition and solid electrolyte interphase revealed by cryogenic transmission electron microscopy. *ACS Nano* **14**, 8766–8775 (2020).
89. Boyle, D. T. et al. Resolving current-dependent regimes of electroplating mechanisms for fast charging lithium metal anodes. *Nano Lett.* **22**, 8224–8232 (2022).
90. He, M., Guo, R., Hobold, G. M., Gao, H. & Gallant, B. M. The intrinsic behavior of lithium fluoride in solid electrolyte interphases on lithium. *Proc. Natl Acad. Sci. USA* **117**, 73–79 (2020).
91. Zhang, X.-Q., Cheng, X.-B., Chen, X., Yan, C. & Zhang, Q. Fluoroethylene carbonate additives to render uniform Li deposits in lithium metal batteries. *Adv. Funct. Mater.* **27**, 1605989 (2017).
92. Dhattarwal, H. S., Kuo, J.-L. & Kashyap, H. K. Mechanistic insight on the stability of ether and fluorinated ether solvent-based lithium bis(fluoromethanesulfonyl) electrolytes near Li metal surface. *J. Phys. Chem. C* **126**, 8953–8963 (2022).
93. Perez-Beltran, S., Kuai, D. & Balbuena, P. B. SEI formation and lithium-ion electrodeposition dynamics in lithium metal batteries via first-principles kinetic Monte Carlo modeling. *ACS Energy Lett.* **9**, 5268–5278 (2024).
94. Tan, Y. et al. Lithium fluoride in electrolyte for stable and safe lithium-metal batteries. *Adv. Mater.* **33**, 2102134 (2021).
95. Zeng, H. et al. Beyond LiF: tailoring Li_2O-dominated solid electrolyte interphase for stable lithium metal batteries. *ACS Nano* **18**, 1969–1981 (2024).
96. Hobold, G. M., Wang, C., Steinberg, K., Li, Y. & Gallant, B. M. High lithium oxide prevalence in the lithium solid–electrolyte interphase for high Coulombic efficiency. *Nat. Energy* **9**, 580–591 (2024).
Correlation of Li_2O prevalence in the SEI and the CE in lithium metal batteries.
97. Gao, K., Sun, L., Wang, K. & Zhang, Y. Non-aqueous liquid electrolytes in lithium metal battery: components and modification. *Mater. Today Energy* **37**, 101413 (2023).
98. Borodin, O., Self, J., Persson, K. A., Wang, C. & Xu, K. Uncharted waters: super-concentrated electrolytes. *Joule* **4**, 69–100 (2020).
99. Jiang, G. et al. Perspective on high-concentration electrolytes for lithium metal batteries. *Small Struct.* **2**, 2000122 (2021).
100. Ren, X. et al. Enabling high-voltage lithium-metal batteries under practical conditions. *Joule* **3**, 1662–1676 (2019).
101. Ren, X. et al. Localized high-concentration sulfone electrolytes for high-efficiency lithium-metal batteries. *Chem* **4**, 1877–1892 (2018).
Introduction of LHCEs as promising electrolyte concept for lithium metal batteries.
102. Zheng, J. et al. Extremely stable sodium metal batteries enabled by localized high-concentration electrolytes. *ACS Energy Lett.* **3**, 315–321 (2018).
103. Efaw, C. M. et al. Localized high-concentration electrolytes get more localized through micelle-like structures. *Nat. Mater.* **22**, 1531–1539 (2023).
104. Verma, A., Schulze, M. C. & Colclasure, A. Micelle-like bulk structure of localized high-concentration electrolytes. *Joule* **8**, 10–12 (2024).
105. Cao, X., Jia, H., Xu, W. & Zhang, J.-G. Review—Localized high-concentration electrolytes for lithium batteries. *J. Electrochem. Soc.* **168**, 010522 (2021).
106. Chen, J. et al. Design of localized high-concentration electrolytes via donor number. *ACS Energy Lett.* **8**, 1723–1734 (2023).
107. Ren, F. et al. Solvent–diluent interaction-mediated solvation structure of localized high-concentration electrolytes. *ACS Appl. Mater. Interfaces* **14**, 4211–4219 (2022).
108. Chen, S. et al. High-voltage lithium-metal batteries enabled by localized high-concentration electrolytes. *Adv. Mater.* **30**, 1706102 (2018).
109. Zhang, X. et al. Advanced electrolytes for fast-charging high-voltage lithium-ion batteries in wide-temperature range. *Adv. Energy Mater.* **10**, 2000368 (2020).
110. Jia, H. et al. High-performance silicon anodes enabled by nonflammable localized high-concentration electrolytes. *Adv. Energy Mater.* **9**, 1900784 (2019).
111. Ahmed, R. A. et al. Enhanced electrochemical performance of disordered rocksalt cathodes in a localized high-concentration electrolyte. *Adv. Energy Mater.* **14**, 2400722 (2024).
112. Cao, X. et al. Optimization of fluorinated orthoformate based electrolytes for practical high-voltage lithium metal batteries. *Energy Storage Mater.* **34**, 76–84 (2021).
113. Cao, X. Effects of fluorinated solvents on electrolyte solvation structures and electrode/electrolyte interphases for lithium metal batteries. *Proc. Natl Acad. Sci. USA* **118**, e2020357118 (2021).
114. Niu, C. et al. Balancing interfacial reactions to achieve long cycle life in high-energy lithium metal batteries. *Nat. Energy* **6**, 723–732 (2021).
115. Perez Beltran, S., Cao, X., Zhang, J.-G., El-Khoury, P. Z. & Balbuena, P. B. Influence of diluent concentration in localized high concentration electrolytes: elucidation of hidden diluent–Li^+ interactions and Li^+ transport mechanism. *J. Mater. Chem. A* **9**, 17459–17473 (2021).
116. Liu, Y. et al. Regulating electrolyte solvation structures via diluent–solvent interactions for safe high-voltage lithium metal batteries. *Small* **20**, 2311812 (2024).
117. Zhao, Y. et al. Electrolyte engineering for highly inorganic solid electrolyte interphase in high-performance lithium metal batteries. *Chem* **9**, 682–697 (2023).
118. Shi, J. et al. An amphiphilic molecule-regulated core–shell-solvation electrolyte for Li-metal batteries at ultra-low temperature. *Angew. Chem. Int. Ed.* **62**, e202218151 (2023).
119. Kim, S. et al. Wide-temperature-range operation of lithium-metal batteries using partially and weakly solvating liquid electrolytes. *Energy Environ. Sci.* **16**, 5108–5122 (2023).
120. Tran, T. et al. Enhancing cycling stability of lithium metal batteries by a bifunctional fluorinated ether. *Adv. Funct. Mater.* **34**, 2407012 (2024).
121. Chen, S. et al. High-efficiency lithium metal batteries with fire-retardant electrolytes. *Joule* **2**, 1548–1558 (2018).
122. Cao, N. et al. Designing ionic liquid electrolytes for a rigid and Li^+-conductive solid electrolyte interface in high performance lithium metal batteries. *Chem. Phys. Lett.* **866**, 141959 (2025).
123. Hai, F. et al. A low-cost, fluorine-free localized highly concentrated electrolyte toward ultra-high loading lithium metal batteries. *Adv. Energy Mater.* **14**, 2304253 (2024).
124. Yuan, Z., Chen, A., Liao, J., Song, L. & Zhou, X. Recent advances in multifunctional generalized local high-concentration electrolytes for high-efficiency alkali metal batteries. *Nano Energy* **119**, 109088 (2024).

125. Li, M. et al. Acetonitrile-based local high-concentration electrolytes for advanced lithium metal batteries. *Adv. Mater.* **36**, 2404271 (2024).
126. Jie, Y. et al. Towards long-life 500 Wh kg^{-1} lithium metal pouch cells via compact ion-pair aggregate electrolytes. *Nat. Energy* **9**, 987–998 (2024).
127. Kim, S. C. et al. High-entropy electrolytes for practical lithium metal batteries. *Nat. Energy* **8**, 814–826 (2023).
128. Li, Z. et al. Critical review of fluorinated electrolytes for high-performance lithium metal batteries. *Adv. Funct. Mater.* **33**, 2300502 (2023).
129. Wichmann, L. et al. Design of fluorine-free weakly coordinating electrolyte solvents with enhanced oxidative stability. *Angew. Chem. Int. Ed.* **64**, e202506826 (2025).
130. Yu, Z. et al. Molecular design for electrolyte solvents enabling energy-dense and long-cycling lithium metal batteries. *Nat. Energy* **5**, 526–533 (2020).
131. Zhang, X. et al. Li^+(ionophore) nanoclusters engineered aqueous/non-aqueous biphasic electrolyte solutions for high-potential lithium-based batteries. *Nat. Nanotechnol.* **20**, 798–806 (2025).
132. Vu, M. C. et al. Low melting alkali-based molten salt electrolytes for solvent-free lithium-metal batteries. *Matter* **6**, 4357–4375 (2023). **Report of low melting FSI-based molten salt electrolyte with high oxidative stability, enabling high Coulombic efficiencies at high rates**.
133. Xue, W. et al. FSI-inspired solvent and 'full fluorosulfonyl' electrolyte for 4 V class lithium-metal batteries. *Energy Environ. Sci.* **13**, 212–220 (2020). **Introduction of full fluorosulfonyl electrolytes for lithium metal batteries**.
134. Xue, W. et al. Ultra-high-voltage Ni-rich layered cathodes in practical Li metal batteries enabled by a sulfonamide-based electrolyte. *Nat. Energy* **6**, 495–505 (2021).
135. Rustomji, C. S. et al. Liquefied gas electrolytes for electrochemical energy storage devices. *Science* **356**, eaal4263 (2017). **Report of liquefied gas electrolytes enabling efficient Li plating/stripping**.
136. Yang, Y. et al. High-efficiency lithium-metal anode enabled by liquefied gas electrolytes. *Joule* **3**, 1986–2000 (2019).
137. Louli, A. J. et al. Diagnosing and correcting anode-free cell failure via electrolyte and morphological analysis. *Nat. Energy* **5**, 693–702 (2020).
138. Weber, R. et al. Long cycle life and dendrite-free lithium morphology in anode-free lithium pouch cells enabled by a dual-salt liquid electrolyte. *Nat. Energy* **4**, 683–689 (2019).
139. Qiu, F. et al. A concentrated ternary-salts electrolyte for high reversible Li metal battery with slight excess Li. *Adv. Energy Mater.* **9**, 1803372 (2019).
140. Kang, D. W., Moon, J., Choi, H.-Y., Shin, H.-C. & Kim, B. G. Stable cycling and uniform lithium deposition in anode-free lithium-metal batteries enabled by a high-concentration dual-salt electrolyte with high $LiNO_3$ content. *J. Power Sources* **490**, 229504 (2021).
141. Stuckenberg, S. et al. Influence of $LiNO_3$ on the lithium metal deposition behavior in carbonate-based liquid electrolytes and on the electrochemical performance in zero-excess lithium metal batteries. *Small* **20**, 2305203 (2024).
142. Agostini, M., Scrosati, B. & Hassoun, J. An advanced lithium-ion sulfur battery for high energy storage. *Adv. Energy Mater.* **5**, 1500481 (2015).
143. Ma, Q. et al. Improved cycling stability of lithium-metal anode with concentrated electrolytes based on lithium (fluorosulfonyl) (trifluoromethanesulfonyl)imide. *ChemElectroChem* **3**, 531–536 (2016).
144. Weintz, D., Kühn, S. P., Winter, M. & Cekic-Laskovic, I. Tailoring the preformed solid electrolyte interphase in lithium metal batteries: impact of fluoroethylene carbonate. *ACS Appl. Mater. Interfaces* **15**, 53526–53532 (2023).
145. Xue, T. et al. Tailoring fluorine-rich solid electrolyte interphase to boost high efficiency and long cycling stability of lithium metal batteries. *Sci. China Chem.* **66**, 2121–2129 (2023).
146. Ding, F. et al. Effects of cesium cations in lithium deposition via self-healing electrostatic shield mechanism. *J. Phys. Chem. C* **118**, 4043–4049 (2014).
147. Ding, F. et al. Dendrite-free lithium deposition via self-healing electrostatic shield mechanism. *J. Am. Chem. Soc.* **135**, 4450–4456 (2013).
148. Frith, J. T., Lacey, M. J. & Ulissi, U. A non-academic perspective on the future of lithium-based batteries. *Nat. Commun.* **14**, 420 (2023).
149. Adams, B. D., Zheng, J., Ren, X., Xu, W. & Zhang, J. Accurate determination of Coulombic efficiency for lithium metal anodes and lithium metal batteries. *Adv. Energy Mater.* **8**, 1702097 (2018).
150. Single, F., Horstmann, B. & Latz, A. Theory of impedance spectroscopy for lithium batteries. *J. Phys. Chem. C* **123**, 27327–27343 (2019).
151. Stolz, L., Winter, M. & Kasnatscheew, J. Practical relevance of charge transfer resistance at the Li metal electrode|electrolyte interface in batteries?. *J. Solid State Electrochem.* **29**, 4181–4186 (2025).
152. Meddings, N. et al. Application of electrochemical impedance spectroscopy to commercial Li-ion cells: a review. *J. Power Sources* **480**, 228742 (2020).
153. Meunier, V., Leal De Souza, M., Morcrette, M. & Grimaud, A. Design of workflows for crosstalk detection and lifetime deviation onset in Li-ion batteries. *Joule* **7**, 42–56 (2023).
154. Meng, W. et al. The progress of *in situ* technology for lithium metal batteries. *Mater. Chem. Front.* **8**, 700–714 (2024).
155. Scurtu, R.-G. et al. From small batteries to big claims. *Nat. Nanotechnol.* **20**, 970–976 (2025).
156. Xu, Y. et al. Atomic to nanoscale origin of vinylene carbonate enhanced cycling stability of lithium metal anode revealed by cryo-transmission electron microscopy. *Nano Lett.* **20**, 418–425 (2020).
157. Cao, X. et al. Monolithic solid–electrolyte interphases formed in fluorinated orthoformate-based electrolytes minimize Li depletion and pulverization. *Nat. Energy* **4**, 796–805 (2019).
158. Chen, W. et al. Formation and impact of nanoscopic oriented phase domains in electrochemical crystalline electrodes. *Nat. Mater.* **22**, 92–99 (2023).
159. Ji, P., Lei, X. & Su, D. In situ transmission electron microscopy methods for lithium-ion batteries. *Small Methods* **8**, 2301539 (2024).
160. Zhang, Z. et al. Characterizing batteries by in situ electrochemical atomic force microscopy: a critical review. *Adv. Energy Mater.* **11**, 2101518 (2021).
161. Wolff, B. & Hausen, F. Mechanical evolution of solid electrolyte interphase on metallic lithium studied by in situ atomic force microscopy. *J. Electrochem. Soc.* **170**, 010534 (2023).
162. Tan, S. et al. Evolution and interplay of lithium metal interphase components revealed by experimental and theoretical studies. *J. Am. Chem. Soc.* **146**, 11711–11718 (2024).
163. Ma, C., Xu, F. & Song, T. Dual-layered interfacial evolution of lithium metal anode: SEI analysis via TOF-SIMS technology. *ACS Appl. Mater. Interfaces* **14**, 20197–20207 (2022).
164. Markevich, E., Salitra, G., Chesneau, F., Schmidt, M. & Aurbach, D. Very stable lithium metal stripping–plating at a high rate and high areal capacity in fluoroethylene carbonate-based organic electrolyte solution. *ACS Energy Lett.* **2**, 1321–1326 (2017).

165. Schmitz, R. et al. SEI investigations on copper electrodes after lithium plating with Raman spectroscopy and mass spectrometry. *J. Power Sources* **233**, 110–114 (2013).
166. Hope, M. A. et al. Selective NMR observation of the SEI–metal interface by dynamic nuclear polarisation from lithium metal. *Nat. Commun.* **11**, 2224 (2020).
167. Hsieh, Y.-C. et al. Quantification of dead lithium via in situ nuclear magnetic resonance spectroscopy. *Cell Rep. Phys. Sci.* **1**, 100139 (2020).
168. Golozar, M. et al. In situ observation of solid electrolyte interphase evolution in a lithium metal battery. *Commun. Chem.* **2**, 131 (2019).
169. Zachman, M. J., Tu, Z., Choudhury, S., Archer, L. A. & Kourkoutis, L. F. Cryo-STEM mapping of solid–liquid interfaces and dendrites in lithium-metal batteries. *Nature* **560**, 345–349 (2018).
170. He, X., Larson, J. M., Bechtel, H. A. & Kostecki, R. In situ infrared nanospectroscopy of the local processes at the Li/polymer electrolyte interface. *Nat. Commun.* **13**, 1398 (2022).
171. Zhang, H., Shen, C., Huang, Y. & Liu, Z. Spontaneously formation of SEI layers on lithium metal from LiFSI/DME and LiTFSI/DME electrolytes. *Appl. Surf. Sci.* **537**, 147983 (2021).
172. Perez Beltran, S. & Balbuena, P. B. SEI formation mechanisms and Li^+ dissolution in lithium metal anodes: impact of the electrolyte composition and the electrolyte-to-anode ratio. *J. Power Sources* **551**, 232203 (2022).
173. Wagner-Henke, J. et al. Knowledge-driven design of solid-electrolyte interphases on lithium metal via multiscale modelling. *Nat. Commun.* **14**, 6823 (2023).
174. Pohlmann, S. Metrics and methods for moving from research to innovation in energy storage. *Nat. Commun.* **13**, 1538 (2022).
175. Benayad, A. et al. High-throughput experimentation and computational freeway lanes for accelerated battery electrolyte and interface development research. *Adv. Energy Mater.* **12**, 2102678 (2022).
176. Ward, L. et al. Principles of the Battery Data Genome. *Joule* **6**, 2253–2271 (2022).
177. Qu, X. et al. The Electrolyte Genome project: a big data approach in battery materials discovery. *Comput. Mater. Sci.* **103**, 56–67 (2015).
178. Tagade, P. M. et al. Attribute driven inverse materials design using deep learning Bayesian framework. *npj Comput. Mater.* **5**, 127 (2019).
179. Barter, D. et al. Predictive stochastic analysis of massive filter-based electrochemical reaction networks. *Digit. Discov.* **2**, 123–137 (2023).
180. Gao, Y.-C. et al. Data-driven insight into the reductive stability of ion–solvent complexes in lithium battery electrolytes. *J. Am. Chem. Soc.* **145**, 23764–23770 (2023).
181. Yan, P. et al. Non-aqueous battery electrolytes: high-throughput experimentation and machine learning-aided optimization of ionic conductivity. *J. Mater. Chem. A* **12**, 19123–19136 (2024).
182. Dave, A. et al. Autonomous optimization of non-aqueous Li-ion battery electrolytes via robotic experimentation and machine learning coupling. *Nat. Commun.* **13**, 5454 (2022).
183. Flores, E. et al. Learning the laws of lithium-ion transport in electrolytes using symbolic regression. *Digit. Discov.* **1**, 440–447 (2022).
184. Lewis, G. N. & Keyes, F. G. The potential of the lithium electrode. *J. Am. Chem. Soc.* **35**, 340–344 (1913).
185. Harris, W. S. *Electrochemical Studies in Cyclic Esters*. PhD thesis, Univ. California, Berkeley (1958).
Demonstration of reversible electrochemical Li deposition and dissolution.
186. Greatbatch, W. et al. The solid-state lithium battery: a new improved chemical power source for implantable cardiac pacemakers. *IEEE Trans. Biomed. Eng* **BME-18**, 317–324 (1971).
187. Peled, E. The electrochemical behavior of alkali and alkaline earth metals in nonaqueous battery systems—the solid electrolyte interphase model. *J. Electrochem. Soc.* **126**, 2047–2051 (1979).
Proposal of the SEI model.
188. Scarr, R. F. Kinetics of the solid lithium electrode in propylene carbonate. *J. Electrochem. Soc.* **117**, 295–298 (1970).
189. Winter, M., Barnett, B. & Xu, K. Before Li ion batteries. *Chem. Rev.* **118**, 11433–11456 (2018).
190. Selim, R. & Bro, P. Some observations on rechargeable lithium electrodes in a propylene carbonate electrolyte. *J. Electrochem. Soc.* **121**, 1457–1459 (1974).
191. Rauh, R. D. & Brummer, S. B. The effect of additives on lithium cycling in propylene carbonate. *Electrochim. Acta* **22**, 75–83 (1977).
192. Koch, V. R. & Young, J. H. The stability of the secondary lithium electrode in tetrahydrofuran-based electrolytes. *J. Electrochem. Soc.* **125**, 1371–1377 (1978).
193. Koch, V. R. & Young, J. H. 2-Methyltetrahydrofuran–lithium hexafluoroarsenate: a superior electrolyte for the secondary lithium electrode. *Science* **204**, 499–501 (1979).
194. Koch, V. R., Goldman, J. L., Mattos, C. J. & Mulvaney, M. Specular lithium deposits from lithium hexafluoroarsenate/diethyl ether electrolytes. *J. Electrochem. Soc.* **129**, 1–4 (1982).
195. Ding, F. et al. Effects of carbonate solvents and lithium salts on morphology and Coulombic efficiency of lithium electrode. *J. Electrochem. Soc.* **160**, A1894–A1901 (2013).
196. Miao, R. et al. Novel dual-salts electrolyte solution for dendrite-free lithium-metal based rechargeable batteries with high cycle reversibility. *J. Power Sources* **271**, 291–297 (2014).
197. Fan, X. et al. Highly fluorinated interphases enable high-voltage Li-metal batteries. *Chem* **4**, 174–185 (2018).
198. Fan, X. et al. Non-flammable electrolyte enables Li-metal batteries with aggressive cathode chemistries. *Nat. Nanotechnol.* **13**, 715–722 (2018).
199. Zhao, Y., Zhou, T., Mensi, M., Choi, J. W. & Coskun, A. Electrolyte engineering via ether solvent fluorination for developing stable non-aqueous lithium metal batteries. *Nat. Commun.* **14**, 299 (2023).
200. Li, C. et al. Developing diluted low-concentration electrolyte with a high anion-to-solvent ratio for high-voltage lithium metal batteries. *J. Mater. Chem. A* **12**, 8236–8243 (2024).
201. Morita, M., Asai, Y., Yoshimoto, N. & Ishikawa, M. A Raman spectroscopic study of organic electrolyte solutions based on binary solvent systems of ethylene carbonate with low viscosity solvents which dissolve different lithium salts. *J. Chem. Soc. Faraday Trans.* **94**, 3451–3456 (1998).
202. Qian, K., Winans, R. E. & Li, T. Insights into the nanostructure, solvation, and dynamics of liquid electrolytes through small-angle X-ray scattering. *Adv. Energy Mater.* **11**, 2002821 (2021).
203. Leifer, N., Aurbach, D. & Greenbaum, S. G. NMR studies of lithium and sodium battery electrolytes. *Prog. Nucl. Magn. Reson. Spectrosc.* **142/143**, 1–54 (2024).
204. Kim, T. et al. Applications of voltammetry in lithium ion battery research. *J. Electrochem. Sci. Technol.* **11**, 14–25 (2020).
205. Hess, S., Wohlfahrt-Mehrens, M. & Wachtler, M. Flammability of Li-ion battery electrolytes: flash point and self-extinguishing time measurements. *J. Electrochem. Soc.* **162**, A3084–A3097 (2015).
206. Hellweg, L., Beuse, T., Winter, M. & Börner, M. Influence of lithium metal deposition on thermal stability: combined DSC and morphology analysis of cyclic aged lithium metal batteries. *J. Electrochem. Soc.* **170**, 040530 (2023).
207. Arbizzani, C., Gabrielli, G. & Mastragostino, M. Thermal stability and flammability of electrolytes for lithium-ion batteries. *J. Power Sources* **196**, 4801–4805 (2011).

Acknowledgements

This Review is the result of a concerted approach within the LILLINT II research project, jointly funded by the US Department of Energy (DOE) and the German Federal Ministry of Research, Technology and Space (BMFTR). A.S. and R.K. acknowledge the financial support of the Assistant Secretary for Energy Efficiency and Renewable Energy, Vehicle Technologies Office (VTO), under the Advanced Battery Materials Research (BMR) Program, of the US DOE under contract DE-AC02-05CH11231. R.A., C.-C.S., X.L. and K.A. acknowledge the US DOE, VTO. Argonne National Laboratory is operated by the DOE Office of Science by UChicago Argonne, LLC, under contract DE-AC02-06CH11357. P.B.B. and J.M.S. acknowledge the US DOE through the US–Germany Cooperation on Energy Storage under contract DE-AC02-05CH11357. Computational resources from the Texas A&M University High Performance Research Computing are gratefully acknowledged. The work performed at Pacific Northwest National Laboratory (PNNL) was supported by the Assistant Secretary for Energy Efficiency and Renewable Energy, VTO, US DOE and the Advanced BMR Program and the US–Germany Cooperation on Energy Storage with contracts DE-LC-000L072 (C.W.) and DE-AC05-76RL01830 (W.X.). Y.S.-H., C.O.P.-R. and D.W. acknowledge the financial support of the Assistant Secretary for Energy Efficiency and Renewable Energy, VTO, under the Advanced BMR Program of the US DOE under contract DE-AC02-06CH11357, subcontract 9F-60231. J.L. and F.S. thank the National Science Foundation for support under grant 2239690. D.C. and F.S. acknowledge the Assistant Secretary for Energy Efficiency and Renewable Energy, VTO, US DOE through the US–Germany Cooperation on Energy Storage under contract DE-AC02-05CH11357. A.U. and U.K. acknowledge the BMFTR in the framework of LILLINT (03XP0511C). Z.L., D.B., M.Werres., B.H. and A.L. acknowledge financial support within the LILLINT II project (03XP0511E). S.W.-M. and B.v.H. acknowledge financial support within the LILLINT II project (03XP0511D). F.H., R.-A.E, S.B., E.F., I.C.-L., D.W. and M.Winter. acknowledge financial support within the LILLINT II project (13XP0511B).

Competing interests

The authors declare no competing interests.

Additional information

Correspondence and requests for materials should be addressed to Rachid Amine, Arnulf Latz, Robert Kostecki or Isidora Cekic-Laskovic.

[1]Forschungszentrum Jülich GmbH, Helmholtz Institute Münster (IMD-4), Münster, Germany. [2]German Aerospace Center (DLR), Institute of Engineering Thermodynamics, Stuttgart, Germany. [3]Helmholtz Institute Ulm for Electrochemical Energy Storage (HIU), Ulm, Germany. [4]Materials Science Division, Argonne National Laboratory, Lemont, IL, USA. [5]Chemical Sciences and Engineering Division, Argonne National Laboratory, Lemont, IL, USA. [6]Energy and Environment Directorate, Pacific Northwest National Laboratory, Richland, WA, USA. [7]Environmental Molecular Sciences Laboratory, Pacific Northwest National Laboratory, Richland, WA, USA. [8]MEET Battery Research Center, University of Muenster, Münster, Germany. [9]Department of Energy and Mineral Engineering and Materials Science and Engineering, The Pennsylvania State University, University Park, PA, USA. [10]Department of Materials Science and Engineering, Massachusetts Institute of Technology, Cambridge, MA, USA. [11]Department of Mechanical Engineering, Massachusetts Institute of Technology, Cambridge, MA, USA. [12]Research Laboratory of Electronics, Massachusetts Institute of Technology, Cambridge, MA, USA. [13]Institute for Applied Materials—Electrochemical Technologies, Karlsruhe Institute of Technology, Karlsruhe, Germany. [14]Department of Chemical Engineering, Texas A&M University, College Station, TX, USA. [15]Department of Materials Science and Engineering, Texas A&M University, College Station, TX, USA. [16]Department of Chemistry, Texas A&M University, College Station, TX, USA. [17]Department of Electrical Engineering, Texas A&M University, College Station, TX, USA. [18]Energy Storage and Distributed Resources Division, Lawrence Berkeley National Laboratory, Berkeley, CA, USA. [19]Karlsruhe Institute of Technology (KIT), Karlsruhe, Germany. [20]Institute of Energy Technologies (IET-1), Jülich, Germany. [21]Institute of Physical Chemistry, RWTH Aachen University, Aachen, Germany. [22]Pritzker School of Molecular Engineering, University of Chicago, Chicago, IL, USA. ✉e-mail: aminer@anl.gov; Arnulf.Latz@dlr.de; r_kostecki@lbl.gov; i.cekic-laskovic@fz-juelich.de